Studies of the mechanisms of amyloid fibril formation with lipid membranes

脂質膜存在下における

アミロイド線維形成メカニズムの解明

A Doctoral Thesis

by

Mayu Terakawa

Submitted to the Graduate School

of Science, Osaka University

August, 2015

Acknowledgement

This work has been performed under the direction of Professor Yuji Goto (Institute for Protein Research, Osaka University). I would like to express my deep gratitude to him for guiding my work with detailed discussion and enthusiastic encouragement.

Thanks to Professor Yasushi Kawata (Tottori University) and his student Naoya Fukui for the supports for experiment with αSN.

I would like to acknowledge Professor Takahiro Sato (Osaka University) and Professor Hiroyasu Yamaguchi for their accepting this dissertation.

This work was supported by the present and past members of the Laboratory of Protein Folding, Institute for Protein Research, Osaka University. I am deeply grateful to Associate Professor Young-Ho Lee and Assistant Professor Hisashi Yagi (Tottori University). Their support and guidance made my thesis work possible. Especially, Associate Professor Young-Ho Lee has been actively interested in my work and has always been available to advise me. I am also grateful to Assistant Professor Masatomo So for giving helpful advices, to Mr. Tatsuya Ikenoue, Mr. Yuxi Lin, Mr. Masayuki Adachi, and Mr. Misaki Kinoshita for helping my experiments and discussion, and to Ms. Kyoko Kigawa, Ms. Miki Hirano, and Mr. Tetsuhei Uenoyama for the assistances of protein expression and purification. I am indebted to all the members of this laboratory for the fruitful discussion and warmhearted encouragements.

I would like to express my very great appreciation to Associate Professor Kazumasa Sakurai (Kinki University), Dr. Yuichi Yoshimura (Aarhus University). I also thank the members of an association of the younger scientists studying biophysics, especially Associate Professor Miho Yanagisawa (Tokyo University of Agriculture and Technology), Dr. Naoto Hori (Maryland University), and Ms. Rina Kagawa (Tokyo University), for helpful advises and encouragement.

I also acknowledge for support from The Research Fellowships of Japan Society for the Promotion of Science for Young Scientists.

Finally, I particularly want to thank my family. My husband, Dr. Tsuyoshi Terakawa (Columbia University), always helps me mentally with discussion and enthusiastic

encouragement. His in-laws, Akira and Eriko Terakawa believe and encourage me. My parents, Shigeru and Masako Suzuki, and my brother, Yuuki, always have supported and encouraged me for a long time. My dog, Megu, soothes me. I have been also encouraged by our new family member during preparing this thesis. I am looking forward to meeting you.

寺川 まゆ

Mayu Terakawa

August 2015

Contents

Abbreviations

Aβ	amyloid β
AFM	atomic force microscopy
ANS	8-anilino-1-naphthalenesulfonate
αSN	α-synuclein
CD	circular dichroism
DOPC	1,2-dioleoyl-*sn*-glycero-3-phosphocholine
DOPE	1,2-dioleoyl-sn-glycero-3-phosphoethanolamine
DOPS	1,2-dioleoyl-*sn*-glycero-3-phospho-L-serine
E. Coli	*Escherichia coli*
ITC	isothermal titration calorimetry
NMR	nuclear magnetic resonance
SUV	small unilamellar vesicle
TEM	transmission electron microscopy
ThT	thioflavin T
TIRFM	total internal reflection fluorescence microscope

Chapter 1. General introduction

1-1. Protein misfolding and amyloid fibrils

The correct folding of unfolded proteins to native structures is essential for their biological functions. However, proteins undergo partial and large denaturation under certain conditions and these processes are often linked to irreversible aggregation. Aberrant aggregation of the peptides and proteins causes a number of neurodegenerative diseases (1). Up to date, approximately 50 disorders have been shown to be associated with the misfolding and aggregation of normally soluble, functional peptides and proteins (2). These disorders have been caused by ageing or lifestyle.

Largely, the types of protein aggregates can be classified depending on the morphology and degree of ordered structure. The aggregates which do not adopt unique conformations are amorphous aggregates. In contrast, the ordered aggregates which contain cross-β structures and are morphologically long in shape are amyloid fibrils. William Astbury, a pioneering biophysicist, stretched a poached egg white into a fiber in the X-ray beam and observed the cross-β fiber diffraction pattern in 1935 (3). Astbury reasoned that, in such fibers, elongated protein strands must be stacked along the fiber axis forming protein sheets that was parallel to each other. In 1968, the characteristic cross-β diffraction pattern was observed when X-rays were directed on amyloid fibers, as Asbury's suggestion (4). This

cross-β diffraction was similar in six different proteins; each one was associated with a different clinical syndrome. Based on these results, the diffuse reflection at 4.8 Å spacing along the vertical shows extended protein chains running roughly perpendicular to the fibril and spaced 4.8 Å apart. The even more diffuse reflection at ~10 Å spacing along horizontal shows that the extended chains are organized into sheets spaced ~10 Å apart (5).

However, amyloid fibrils with large molecular sizes are inherently noncrystalline and insoluble materials. Thus, these natures still hamper the determination of internal molecular structures of amyloid fibrils by traditional methods with high resolution such as X-ray crystallography and multidimensional nuclear magnetic resonance (NMR) spectroscopy. Over 10-15 years, their internal molecular structures have been investigated through the application of less traditional methods. One of the most powerful methods is solid-state NMR (ssNMR) spectroscopy. ssNMR with various pulse sequences which are tailored for molecular assemblies has shown its application to insoluble and non-crystalline aggregates (6). Detailed structural information at the molecular level is essential for understanding the underlying mechanism of the amyloid formation and help to the drug design.

The whole fibrillar self-assembly process is divided to the two processes:

nucleation and elongation steps. The formation of transient nuclei is a rate-limiting step, thus it takes a time. On one hand, the elongation step occurs rapidly. Amyloid fibrils can be detected by the fluorescent agents such as Congo red and thioflavin T (ThT). ThT is the most widely used to assay amyloid fibrils since it produces a strong fluorescence by binding to amyloid fibrils (7). Therefore, ThT-based kinetic observation on the formation of amyloid fibrils is mostly popular. As shown in Fig. 1, the period where ThT fluorescence does not show the increase in the intensity in an earlier stage represents the nucleation step, and the middle part where ThT fluorescence increases indicates the elongation step. The last plateau phase shows the stationary states where the elongation reaction is finished.

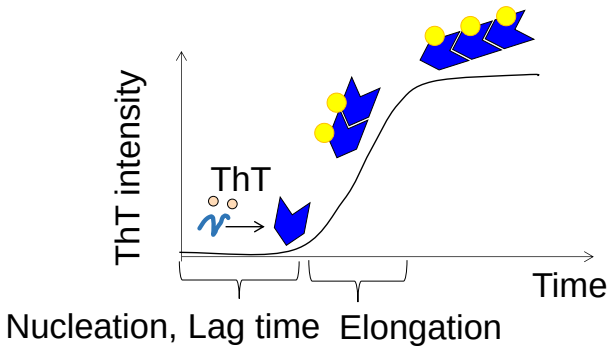

FIGURE 1. Typical kinetics of amyloid formation. Monomers of amyloidogenic proteins are dissolved in solution. ThT is not bound to monomers. It takes a time to form nuclei, and this term is called nucleation reaction. Followed by lag time, elongation reaction is started. ThT is bound to elongating fibrils. After elongation reaction, monomers were depleted and intensity of ThT becomes plateau.

1-2. Interactions between amyloid-forming proteins and membranes

Many researchers have tried to demonstrate the mechanisms of the fibrillation using a variety of amyloid-forming proteins. They found that the fibrillation occurred due to several reasons including suppression of diffusion, solubility limit, and physicochemical and conformational property of proteins (8-10). The concentration of proteins *in vivo* is normally much lower than that for *in vitro* experiments. Thus, researchers searched for biologically relevant factors which induced amyloid fibrillation *in vivo* and started to focus on the role of lipid membranes. Since lipid membranes condense proteins which increases the effective concentration, e.g., decreasing solubility, and reduces the diffusional dimension of the proteins from three to two dimensions (11,12). Binding of amyloidogenic proteins to lipid membranes also induces conformational changes of proteins. For example, amyloid β (Aβ) peptides (Fig. 2*a*), which are the main constituents of the senile plaques in the brains of Alzheimer's disease patients, were bound to membranes containing GM1, one of glycolipids, and the formation of amyloid fibrils of Aβ peptides was markedly enhanced (13). Intrinsically disordered α-synuclein (αSN) (Fig. 2*b*), of which accumulations are responsible for Parkinson's disease, changed the conformation to an extended α-helix. Interestingly, the conformational transitions depended on the surface curvature and charge of the membranes

(14,15).

FIGURE 2. Amino acid sequence of Aβ and αSN. Primary amino acid sequence of Aβ (1-42) (a) and αSN (b).

1-2-1. Interactions between amyloid β and membranes

In vivo, Aβ peptides consist of 39-42 residues and are produced by sequential cleavage of the transmembrane amyloid precursor protein (APP) by β- and γ-secretase (16,17). The difference in the length of Aβ peptides depends on the cleavage site by γ-secretase. The most typical types are Aβ (1-40) and Aβ (1-42) peptides, which consist of 40 and 42 amino acids, respectively. These peptides contain six positively charged residues, six negatively charged residues, and hydrophobic residues in the C terminal part. The Aβ (1-40) and Aβ (1-42) peptides are found on the senile plaque and Aβ (1-42) peptides are reported to be more toxic than Aβ (1-40) peptides (18).

The concentration of Aβ peptides *in vivo* is about a few nM (9,17,19,20). However, the fibrillation of Aβ peptides *in vitro* requires more than a few μM (21,22). To resolve this discrepancy, lipid membranes were focused. Yanagisawa and coworkers reported that Aβ peptides bound to GM1 accelerated the formation of amyloid fibrils (13). Subsequently to this study, a lot of researchers examined the interaction between Aβ peptides and membranes. Matsuzaki and colleagues suggested that the binding of Aβ peptides to GM1-containing membranes induced a transition from random coil to α-helix at the low peptide/lipid ratio (23). At the high ratios, the membranes promoted the transition to β-sheet-rich conformations,

which indicated the formation of amyloid fibrils due to the acceleration of nucleation on membranes. Meanwhile, using model membranes, other studies showed that the propensity and mechanism of aggregation of the amyloidogenic protein and peptide depended on the component of lipids (12). Physicochemical properties of constituent lipids were found to be an important factor for determining a pathway of aggregation of proteins.

One of the most critical physical features of the membranes in living cells is curvature which has been less focused in some protein misfolding and aggregation. Depending on the degree of curvature, it was conceivable that the binding mode and conformational transitions of proteins on membranes or nucleation could be altered. Therefore, I focused on the effect of a curvature of the membranes on the fibrillation of Aβ (1-40) peptides. In the chapter 2, I showed that the membrane curvature was one of the key factors to control amyloidogenesis of Aβ (1-40) peptides.

1-2-2. Interactions between α-synuclein and membranes

α-Synuclein (αSN) is divided into the three main regions on the basis of the physicochemical property of amino acid residues: 1) the N-terminal region, which is amphipathic in nature and contains a lot of positive charges at neutral pH. The N-terminal region plays a central role in binding to membrane surfaces with a conformational shift to an α-helical structure; 2) non-amyloid β component (NAC) region, which displays a high tendency to aggregate into amyloid fibrils with high local hydrophobicity; 3) the C-terminal region, which is highly negatively charged (24).

The N-terminal region has shown its capability of binding to negatively charged small vesicles such as vesicles which mimicked (pre)synaptic vesicles. αSN was found around the synaptic vesicle and nuclear membrane in cells (25,26). Accordingly, synuclein was named after the property of the localization in cells. Despite of extensive endeavors, biological functions of αSN still remain unclear.

Although the localization of αSN around nuclear membrane is needed to be more obvious, a line of compelling evidence showed the presence of αSN around synaptic vesicles. In this context, active studies on the interactions between αSN and synaptic vesicles has been progressed (27). To mimic the membranes of synaptic vesicles *in vitro*, small unilamellar

vesicles (SUV) containing phosphatidylcholine (PC), phosphatidylethanolamine (PE), and phosphatidylserine (SE) were used. It was reported that αSN, bound to this vesicles, changed the conformation from random coil to α-helical structures and it was suggested that helical structures were intermediates along the pathway of amyloid formation (28). However, membrane-bound α-helical structures are thermodynamically stable states (29,30). Therefore, it can be also rationalized that the transition of α-helical structures on the membranes to β structures of amyloid fibrils are not easy as generally expected.

In order to answer this question, in the chapter 3, I examined the interactions of αSN with the two types of SUVs: one is presynaptic vesicle mimicking (mimic) SUVs and the other is SUVs which consisted of DOPC lipids for control. Then, I investigated the conformational transition of disordered αSN to other structural states. Treatment of ultrasonication, which promotes the formation of amyloid fibrils (31,32), was simultaneously introduced to form amyloid fibrils of αSN.

Considering the pathological and biological relevance, I further utilized the mutant (αSN_{A53T}) of familial Parkinson's disease and two C-terminal truncation mutants (αSN_{103} and αSN_{129}). Moreover, to verify the importance of the charge in C-terminal region in the initial conformational states and fibrillation propensity, I also introduced a charge-neutralized

mutant (αSN_{NC}). I showed that the degree of α-helix depended on the concentration of lipids of mimic SUVs and was important for regulating amyloidogenicity of αSN.

Chapter 2. Small liposomes accelerate the fibrillation of amyloid β (1-40)

2-1. Introduction

Alzheimer's disease is one of the most deleterious neurological diseases. The main cause of this disease has been attributed to the deposition of amyloid β (Aβ) peptides in the brain (8,22,33); therefore, a large number of studies have examined the mechanism underlying the fibrillation of Aβ peptides *in vivo* and *in vitro*. Aβ peptides are produced by the sequential cleavage of the amyloid precursor protein with β and γ secretases. Although Aβ peptides are initially disordered in solution, they fold to form an oligomeric nucleus, possibly with a large amount of cross-β structures. Elongation then occurs, resulting in the formation of mature amyloid fibrils (18,22,34). The structures and toxicities of oligomers, which are directly responsible for cytotoxicity, were the recent targets of studies on Alzheimer's disease as well as other amyloidosis (35). In a previous study using NMR, it was reported that one of the initial structures of oligomers was a non-β-sheet structure containing 3-10 helix in solution (36).

Aβ peptide concentrations *in vivo* were shown to be a few nM (~5 nM) (9,17,19,20), whereas fibrillation *in vitro* requires an order of magnitude higher concentration (21,22). To clarify the reason for this difference, many studies proposed that Aβ peptides might interact with lipid membranes, which decreases diffusional dimensions and increases the local

concentration of Aβ peptides (13,37,38). Various studies showed that specific membrane components (e.g. cholesterol, sphingomyelin, ganglioside, etc.) interact specifically with Aβ peptides, and this interaction has an important role in Aβ fibrillation (13,39-43); however other studies challenged this proposal (44,45). Recently, a two-step mechanism of membrane disruption by Aβ peptides has been proposed, in which (i) Aβ oligomers bind to the membrane to form ion permeable pores and (ii) the process of Aβ fibrillation causes membrane disruption mainly due to the interaction of Aβ fibrils with gangliosides (43,46).

Amyloid fibrillation of various proteins, other than Aβ peptides, in lipid membranes has been extensively studied. Lipid membranes are known to be involved in the fibrillation of α-synuclein and human islet amyloid polypeptide, which are associated with Parkinson's disease and type 2 diabetes, respectively (14,47-49). Various kinds of lipids that affect amyloid fibrillation have also been studied, and the findings obtained revealed that electrostatic interactions between proteins and membranes facilitated the binding of proteins to the membranes as well as their fibrillation (14,50,51). The size or radius of liposomes may also be an important factor for determining these interactions: α-synuclein binds to small unilamellar vesicles and islet amyloid polypeptide interacts with highly-curvature membranes (52-54).

However, the role of membrane properties on the fibrillation of Aβ peptides has not yet been elucidated in detail. Previous studies using giant unilamellar vesicles of 1,2-dioleoyl-*sn*-glycero-3-phosphocholine (DOPC) suggested that Aβ peptides binding caused membrane deformation (55,56). A simulation study revealed that the accumulation of Aβ peptides deformed membranes to produce highly curved membranes (57).

Thus, the deformation of membranes may be one of the key factors that accelerate fibrillation. Moreover, the presence of Aβ peptides in the synapses *in vivo* caused a dysfunction in synaptic vesicles with a diameter of approximately 40 nm (58). Because the binding of Aβ peptides to a membrane and the subsequent deformation is a linked phenomenon, the presence of deformed membranes may accelerate the binding and fibrillation of Aβ. Membrane curvature, one possible type of membrane deformation, can be controlled by changing the radius of liposomes; therefore, studies are needed to verify the relationship between membrane deformation, binding, and fibrillation.

I herein examined the effects of liposomes of various diameters on the amyloid fibrillation of Aβ (1-40) in order to determine whether the fibrillation depends on the membrane curvature and consequent increase in water-accessible hydrophobic regions. I chose DOPC and 1-palmitoyl-2-oleoyl-*sn*-glycero-3-phosphocholine (POPC) as the liposome

components, because Aβ binding was reported to bend phosphocholine membranes (57) and phosphocholine, a zwitterionic lipid, allowed us to focus on the effects of membrane curvature while minimizing the effects of electrostatic interactions (39,59). It was previously observed that, although Aβ (1-40) is relatively easy to keep in monomeric states, Aβ (1-42) forms nuclei for spontaneous fibrillation much faster than Aβ (1-40) (60). Consequent explosive fibrillation of Aβ (1-42) resulted in a large number of short fibrils, minimizing the interaction with the surface. Thus, to address the effects of membranes, I chose Aβ (1-40), although it will be important to compare Aβ (1-40) and Aβ (1-42) to obtain further insight into the interactions of Aβ with membranes.

The results of the present study revealed that membrane curvature is an important factor for determining the amyloid fibrillation of Aβ (1-40). Liposomes of larger sizes decreased the length of amyloid fibrils, and this was accompanied by an increase in the amount of amorphous aggregates. These results suggest that amyloid fibrillation on membranes competes with amorphous aggregation, thereby providing an insight into the mechanism underlying synaptic vesicle impairments.

2-2. Experimental procedure

***Materials*—**Lyophilized Aβ (1–40) purchased from Peptide Institute Inc. (Osaka, Japan) was dissolved in a 0.05% (w/w) ammonia solution at a concentration of 100 μM and stored at −80 °C. Phospholipids: DOPC, POPC, 1,2-dioleoyl-*sn*-glycero-3-phospho-L-serine (DOPS), and 1,2-dioleoyl-*sn*-glycero-3-phosphoethanolamine-N-(lissamine rhodamine B sulfonyl) (Rho-DOPE) were purchased from Avanti Polar Lipids Inc. (Alabaster, AL). Thioflavin T (ThT) and 8-anilino-1-naphthalenesulfonate (ANS) were obtained from Wako Pure Chemical Industries Ltd. (Osaka, Japan) and Sigma-Aldrich Co. (St. Louis, MO) respectively. All other reagents were obtained from Nacalai Tesque (Kyoto, Japan).

***Preparation of liposomes*—**Liposomes were prepared as previously described (61). Briefly, lipids (~10 mM) were stored in methanol stock solutions. Lipid films were prepared by drying appropriate amounts of the stock solution in a stream of dry nitrogen, followed by desiccation for at least 1 h to ensure removal of the organic solvent. Appropriate buffer solutions were added and vortexed to rehydrate the lipid films. After ten freeze-thaw cycles, lipid suspensions were extruded 20 times through 50-, 100-, or 200-nm polycarbonate membranes (Whatman, Clifton, NJ) using a miniextruder (Avanti Polar Lipids, Inc., Alabaster, AL) just before use. Liposomes with a diameter of 30 nm were prepared by an ethanol

injection method with slight modifications (62). Appropriate lipids (~100mM) in methanol were diluted to 10% (v/v). After vortexing, the lipid suspension in the tubes were set on a water bath-type ultrasonic transmitter with a temperature controller (ELESTEIN SP070-PG-M, Elekon Sci. Inc., Chiba, Japan), which applied repetitive ultrasonication pulses to samples from three directions (63). The temperature was set to 37 °C and ultrasonic pulses were applied with repeats of 1 min ultrasonication and 9 min quiescence for 3 h. After ultrasonication, this suspension was centrifuged to precipitate multilamellar liposomes or/and aggregations of lipids followed by the collection of the supernatant. As this supernatant may contain methanol, it was dialyzed against an appropriate buffer twice. After dialysis, the concentration of lipids was quantified. Liposome sizes were measured by dynamic light scattering using DynaPro Titan (Wyatt Technology Co., Goleta, CA), using vesicles of 100 μM DOPC. Liposomes containing the fluorescence lipid (Rho-DOPE) (0.1% mol) or DOPS were prepared using the same procedure as described above.

Analytical ultracentrifugation—The sedimentation velocity data were obtained by a Beckman-Coulter Optima XL-A analytical ultracentrifuge (Beckman Coulter, Miami, FL). The samples were first centrifuged at 3,000 rpm (700 g) for 5 min to stabilize the absorbance and temperature. Next, centrifugation was performed at 60,000 rpm (250,000 g) and 4 °C.

Absorbance data at 220 nm were collected at an interval of 20 min at the radial increment of 0.003 cm in the continuous scanning mode. The absorbance data were analyzed by using sedfit (http://www.analyticalultracentrifugation.com/default.htm) to obtain the sedimentation coefficients. The parameters of solvent conditions (partial specific volume, density and viscosity) were calculated by using sednterp (http://sednterp.unh.edu/#).

Total internal reflection fluorescence microscopy (TIRFM), atomic force microscopy (AFM), and transmission electron microscopy (TEM)—The prism-type TIRFM system was used to observe individual amyloid fibrils. The details of this system were described previously (64,65). Briefly, an aliquot (14 μl) of sample solution was deposited on a quartz glass slide, and a fibril image was obtained with TIRFM. I used an Ar laser (532 nm) and a He-Cd laser (442 nm) to excite ThT and rhodamine, respectively. AFM images were obtained using a Digital Instruments Nanoscope IIIa scanning microscope (Veeco Instruments Inc., Plainview, NY) as reported previously (66). TEM images were obtained using a HITACHI H-7650 transmission microscope (Hitachi, Tokyo, Japan) at 20 °C with a voltage of 80 kV and magnification of 30,000. The sample solution (5 μl) was spotted onto a collodion-coated copper grid (Nisshin EM Co., Tokyo, Japan). After 1 min, the remaining solution was removed with filter paper and 5 μl 2 % (w/w) uranyl acetate was spotted onto

collodion-coated copper grids. After 1 min, the remaining solution was removed in the same manner.

Amyloid fibrillation and ThT fluorescence assay—The formation of Aβ (1-40) fibrils was examined at 10 μM in 10 mM sodium phosphate buffer (pH 7.5) containing 5 μM ThT, 100 mM NaCl, and DOPC or POPC liposomes at various concentrations. These solutions (200 μl) were added to the 96-wells microplates (Greiner-Bio-One, Tokyo, Japan) and a seal was affixed (PowerSeal CRISTAl VIEW, Greiner-Bio-One, Tokyo, Japan). The plates were set on a microplate reader (SH-9000, Corona Electric Co., Ibaraki, Japan) and amyloid fibrillation was monitored by ThT fluorescence. It is noted that, although the morphology of Aβ fibrils is likely to depend on agitation of solution (67), I used the fibrillation conditions without agitation. The fluorescence intensity of ThT at 490 nm was measured with an excitation wavelength of 450 nm at 37 °C. The lag time of fibrillation was defined as the time at which ThT fluorescence reached 10% of the maximum.

ANS assay to evaluate hydrophobicity—ANS fluorescence was measured using the Hitachi fluorescence spectrophotometer F4500 with the excitation wavelengths at 350 nm. The fluorescence of ANS was monitored by adding 2 μM ANS to the solution. The concentrations of liposomes and amyloid fibrils were 2 μM, respectively.

Isothermal titration calorimetry—Isothermal titration calorimetry (ITC) of Aβ (1-40) monomers to the two different sizes of DOPC liposomes (30 nm and 100 nm) in 10 mM phosphate buffer (pH 7.5) containing 100 mM NaCl was performed by using a VP-ITC instrument (GE-Healthcare, Waukesha, WI) at 37 °C. The concentrations of Aβ (1-40) in the syringe and liposomes in the cell were 100 μM and 5 mM, respectively. The reference power for the baseline was set to 10 μcal/s and the initial delay was 1800 s. Titration of Aβ (1-40) was comprised of 23 injections with the spacing time of 900 s or 300 s and the filter period of 2 s. The injection volume was 12 μL for each and the stirring speed was 242 rpm.

The heat of dilution (and mixing) of Aβ (1-40) titrated to the same buffer was also measured. The apparent values of the change in enthalpy ($^{app}\Delta H_{bind}$) and the association constant ($^{app}K_a$) were obtained by the fit of the binding isotherms to the one-site binding model incorporated in Origin 7.1. By using the following relationships, $^{app}\Delta G_{bind} = -RT \ln(^{app}K_a) = {}^{app}\Delta H_{bind} - T\,{}^{app}\Delta S_{bind}$, the apparent thermodynamic values of the change in Gibbs free energy ($^{app}\Delta G_{bind}$) and entropy ($^{app}\Delta S_{bind}$), were further calculated. The apparent dissociation constant ($^{app}K_d$) was obtained based on the relation of $^{app}K_a = 1/{}^{app}K_a$. It should be noted that $^{app}\Delta H_{bind}$ values are more susceptible to the fit than $^{app}K_a$ values.

2-3. Results

Preparation of liposomes and Aβ solution

To investigate the effects of the liposome size on the fibrillation of Aβ (1-40), I prepared liposomes of four sizes (~ 200, 100, 50, and 30 nm) and analyzed the kinetics of fibrillation monitored by ThT fluorescence. I first confirmed the size of DOPC liposomes with TEM (Fig. 1*a*-*d*) and dynamic light scattering (Fig. 1*e*-*h*). The results obtained indicated that I could prepare liposome samples of distinct sizes with relatively small distributions. I call the respective preparations 30, 50, 100, and 200 nm liposomes.

To check whether Aβ (1-40) samples before the fibrillation experiments were monomeric, I conducted a sedimentation velocity measurement (Fig. 1*i*, *j*). The sedimentation coefficient distribution for Aβ (1-40) solution revealed a sharp peak at ~0.3 S. Using this value, I calculated the molecular weight to be ~4,700, consistent with that of Aβ (1-40) monomer, 4,300.

The absence of oligomeric aggregates was further confirmed by native-PAGE followed by Western blotting with antibodies to Aβ (1-40) monomers (data not shown). In addition, I observed the kinetics of Aβ (1-40) fibrillation with samples with and without ultracentrifugation to remove possible aggregates, where I also checked the effects of 30 and

100 nm liposomes. I did not observe significant differences between Aβ (1-40) samples with and without ultracentrifugation (data not shown). Therefore, I used Aβ (1-40) preparations without ultracentrifugation assuming that I can address fibrillation of Aβ (1-40) monomers.

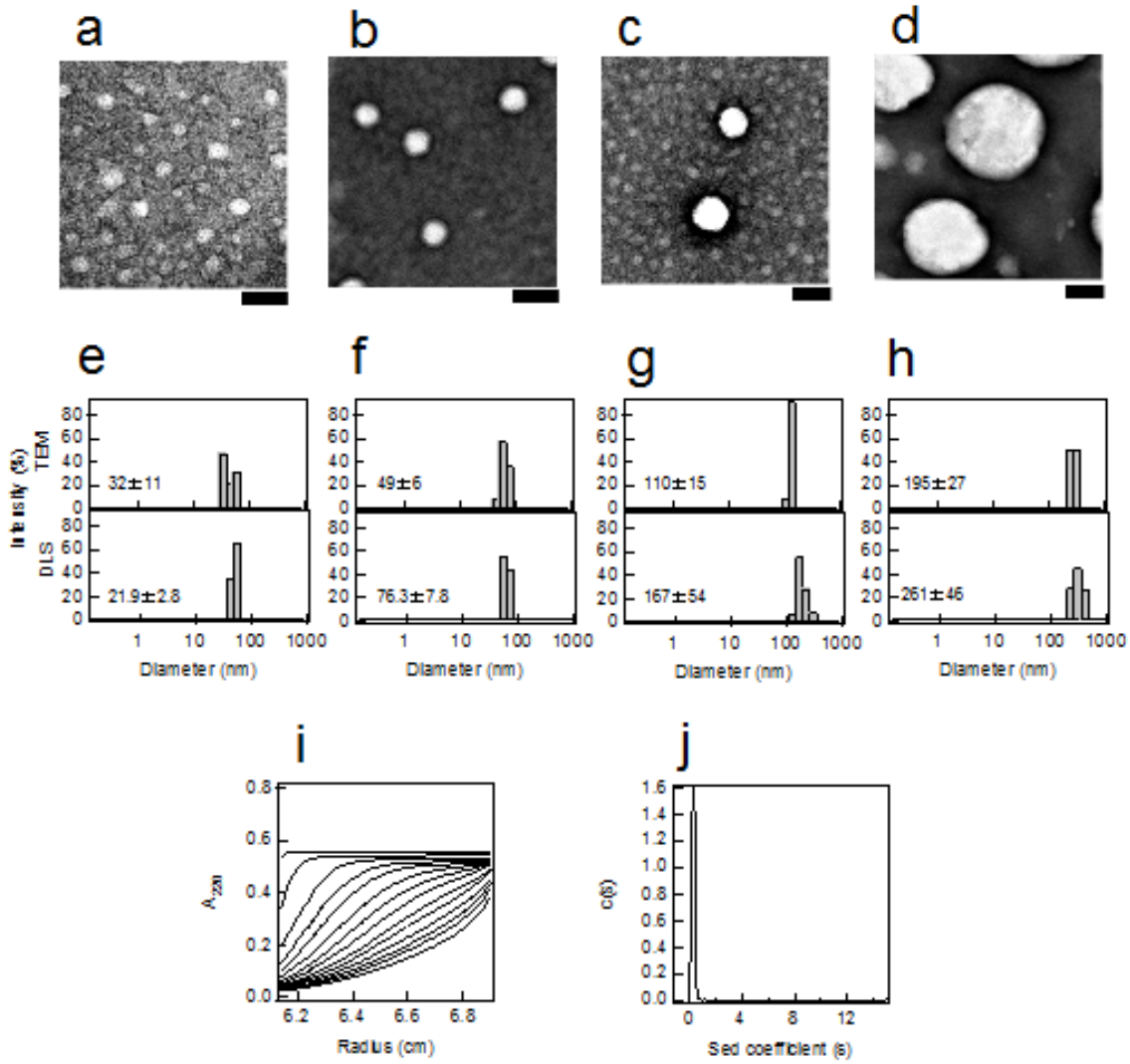

FIGURE 1. Preparation of liposomes of various sizes and Aβ monomers. (*a-d*) TEM images of liposomes of various diameters: 30 (*a*), 50 (*b*), 100 (*c*), and 200 nm (*d*). The scale bar represents 100 nm. (*e-h*) Distribution of liposome diameters determined by TEM and dynamic light scattering. The liposome diameters prepared were 30 (*e*), 50 (*f*), 100 (*g*), and 200 (*h*) nm. (*i*) Sedimentation boundary profiles of Aβ monomers. Sedimentation pattern was recorded at 60,000 rpm and 4 °C by monitoring the absorbance at 220 nm, and fitted traces at intervals of 20 min are shown. (*j*) Sedimentation coefficient distributions derived from sedimentation boundary profiles of Aβ monomers.

Dependence of fibrillation on the liposome concentration

I monitored the fibrillation of 10 μM Aβ (1-40) in 10 mM phosphate buffer (pH 7.5) containing 100 mM NaCl and 5 μM ThT at 37°C using amyloid-specific ThT fluorescence (7). It has been reported that Aβ (1-40) fibrils with twofold symmetry with twisted morphology predominate when fibrils are grown in vitro with agitation of the Aβ (1-40) solution, while fibrils with three-fold symmetry with straight ribbon morphology predominate when fibrils are grown without agitation (67). Throughout the paper, I prepared the fibrils without agitation, because agitation might affect the morphologies of liposomes.

Spontaneous fibrillation without agitation occurred with a lag time of 12 h (Fig. 2*a*). The straight and long morphology of mature fibrils was confirmed by TIRFM, AFM, and TEM (see below). These results were consistent with the findings of the previous studies (60,68).

To examine the effects of liposomes on the fibrillation of 10 μM Aβ (1-40), I added 30 or 100 nm liposomes at 10, 50, 100, 250, 500, 750, and 1000 μM (Fig. 2*a*, *d*). I observed a significant acceleration in fibrillation in the presence of 30 nm liposomes at 10 μM, as revealed by a decrease in the lag time from ~12 h to ~7.6 h (Fig. 2*a* inset): The relative lag time in 30 nm liposomes at 10 μM was 0.6 (Fig. 2*b*). Further increases in the liposome

concentration slightly decreased the lag time. I compared the amount of fibrils by the ThT intensities at the end of the measurements (i.e. final ThT intensities at about 40 h). When the ThT intensity decreased after the maximum, I used the maximal ThT intensity. The final ThT intensity was similar to that in the absence of liposomes at all the liposome concentrations examined (Fig. 2*c*). In contrast, the presence of 100 nm liposomes at various concentrations slightly decreased the lag time (Fig. 2*d* inset and 2*e*). The final ThT intensity in the presence of 100 nm liposomes was independent of the liposome concentration within an acceptable level of error (Fig. 2*f*).

These results suggested that 10 μM liposomes were sufficient to examine the effects of liposomes on the fibrillation of 10 μM Aβ (1-40). The binding equilibrium between Aβ (1-40) and liposomes that affected amyloid fibrillation may have been established even at low concentrations of liposomes. Thus, I used 10 μM DOPC liposomes to examine the effects of liposomes of various sizes on the fibrillation of Aβ (1-40).

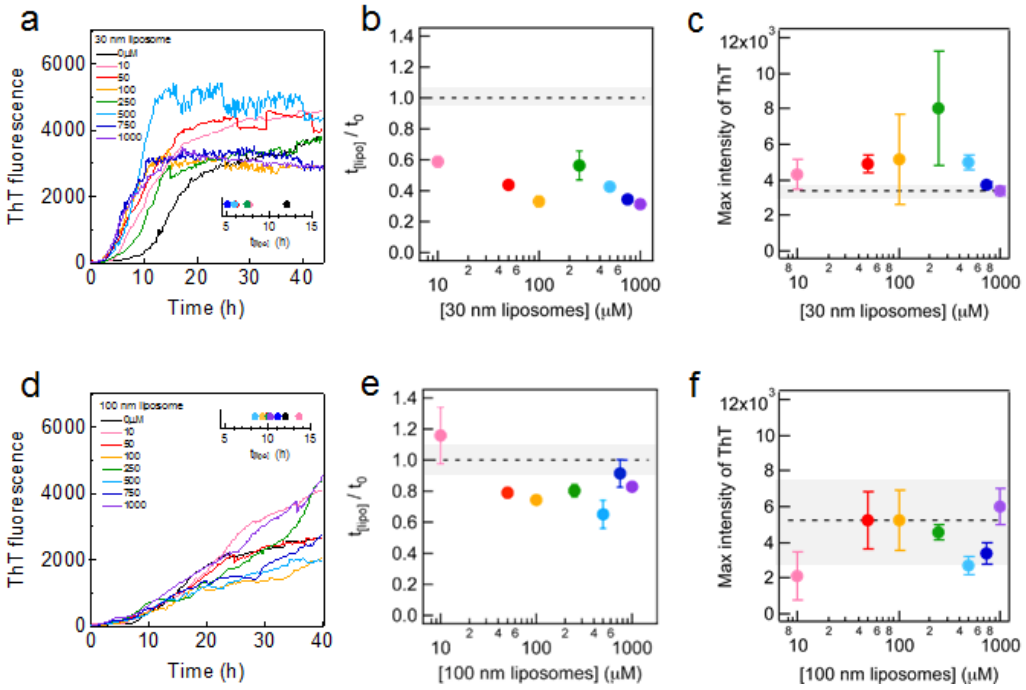

FIGURE 2. Effects of 30 and 100 nm DOPC liposomes on amyloid fibrillation of Aβ (1-40) at 37 °C without shaking. (*a*,*d*) Kinetics monitored by ThT fluorescence in the absence and presence of 30 nm (*a*) or 100 nm (*d*) DOPC liposomes at various concentrations at 37 °C. The concentrations of the liposomes are described in each figure. Amyloid fibrillation at the respective liposome concentrations was monitored at three wells and the representative kinetics is shown. The insets show the average lag times. Black dots and dots with the other colors indicate the average lag time without lipids (t_0) and with liposomes ($t_{[lipo]}$), respectively. (*b*, *c*, *e*, *f*) Dependencies of the relative lag time (*b*, *e*) and maximal ThT amplitude (*c*, *f*) on the 30 nm (*b*, *c*) or 100 nm (*e*, *f*) DOPC liposome concentrations. Dotted lines are the values obtained in the absence of liposomes. The error bars and grey zones indicate the standard deviation among three experiments.

Dependence of fibrillation on the liposome size

The kinetics of Aβ (1-40) fibrillation was examined in the presence of 10 μM DOPC liposomes of various diameters (i.e. 30, 50, 100, and 200 nm) (Fig. 3*a*). The size of DOPC liposomes notably affected both the lag time and final ThT intensity (Fig. 3*c*, *d*). The lag time was the shortest for the 30 nm liposomes, and increased with the size of liposomes, returning back to the value in the absence of liposomes at 100 or 200 nm liposomes (Fig. 3*a inset, c*). On the other hand, the maximal ThT intensities observed in the presence of 30 or 50 nm liposomes were similar to that in the absence of liposomes and were larger than those in the presence of 100 or 200 nm liposomes (Fig. 3*d*). The slope of the elongation process after the lag time was slightly less steep in the presence of 100 or 200 nm DOPC liposomes (Fig. 3*a*). These results suggested that small liposomes accelerated fibrillation without changing the final amount of fibrils, while the larger liposomes decreased the amount of fibrils without an apparent decrease in the fibrillation rate.

I performed the same experiments with POPC liposomes at 10 μM (Fig. 3*b*). Both the lag time and final ThT intensity revealed similar dependencies on the size of liposomes to those observed for DOPC liposomes (Fig. 3*b inset, c,* and *d*), although the final ThT intensities of POPC liposomes were smaller than those of DOPC liposomes. The smaller final

ThT intensities of POPC liposomes might be caused by the difference of the membrane surface properties due to the difference of acyl chains or of the temperature of gel-liquid crystalline phase transition: Transition temperatures are -17 and -2 °C for DOPC and POPC membranes, respectively. Although there were some differences between DOPC and POPC, I could observe a similar effect of liposome size on the kinetics of Aβ (1-40) fibrillation. These results suggested that the size-dependent effects of liposomes might be common to various liposomes. I then attempted to address why 30 and 50 nm liposomes significantly promoted the nucleation reaction while larger liposomes reduced the maximal ThT value without notable effects on the lag time.

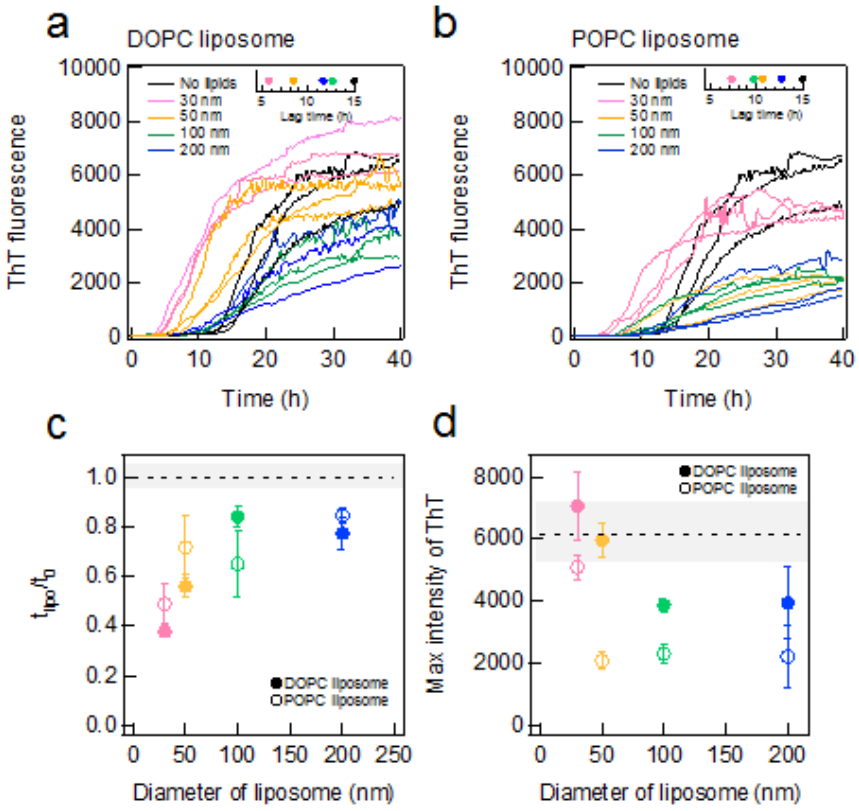

FIGURE 3. Effects of liposomes of various sizes on Aβ amyloid fibrillation. (*a, b*) Kinetics monitored by ThT fluorescence in the absence (black) or presence of DOPC (*a*) or POPC (*b*) liposomes of 30 (pink), 50 (yellow), 100 (green), or 200 nm (blue) at 37 °C without shaking. Liposome and Aβ concentrations were 10 μM. The insets show the average lag times. (*c, d*) Dependencies of the relative lag time (*c*) and maximal ThT amplitude (*d*) on the liposome size. Dotted lines are the values obtained in the absence of liposomes. The error bars and grey zones indicate the standard deviation among three experiments.

Hydrophobic surface of membranes exposed to a solvent

In order to clarify the mechanism underlying the promotion of nucleation by small liposomes, I assumed that Aβ (1-40) interacted preferentially with the parts of membranes where water molecules could penetrate. The penetration depth of water representing water-accessible hydrophobic regions may depend on the size of the liposomes and may be larger (deeper) for small size liposomes. Smaller liposomes (≤ 50 nm) may have more of these regions than larger liposomes. A previous study reported that the insertion of the C-terminus of Aβ peptides that contained a series of hydrophobic amino acids into membranes was crucial to the structural conversion of monomeric Aβ peptides to amyloid fibrils (69). Moreover, the interface between the head groups and acyl chains of lipids was shown to be responsible for the binding and conformational conversion of Aβ peptides (70,71). Hence, a more detailed characterization of the relationship between the kinetics of Aβ fibrillation and hydrophobicity of liposomes will be important.

To examine this hypothesis, I assessed the water-accessible hydrophobic surface of liposomes by measuring ANS fluorescence at 2 μM in the presence of various sizes of DOPC liposomes at 2 μM (Fig. 4*a*). ANS is a hydrophobic dye, the fluorescence of which increases markedly in a hydrophobic environment, and is often used to detect water-accessible

hydrophobic regions in the intermediates of protein folding (72). Using this assay, I speculated that I might be able to detect the exposure of the hydrophobic groups (i.e. acyl chains) of membranes.

The fluorescence intensity of ANS was low at a maximum of 520 nm in the absence of liposomes (Fig. 4*a*). The fluorescence of ANS increased, following the addition of 30 nm liposomes at 2 μM, with a blue shift being observed in the maximum to 500 nm, which suggested the partial burial of the dye in a hydrophobic environment. The increase observed in ANS fluorescence and the blue shift were less for larger liposomes. (Fig. 4*a, b*). These results indicated that the water-accessible hydrophobic regions (or solvent penetration) depended on the size of liposomes: smaller liposomes exposed more hydrophobic regions to the solvent than larger liposomes.

To address the dependence of ANS fluorescence on the liposome size, I calculated the distance between two head groups of lipids, *d*. As shown in Fig. 4*c*, I assumed a simplified model in which the inner leaflet was ignored and the lipid of the outer leaflet was represented by a rectangular parallel piped. According to this model, the inside circumference was $\pi(R\text{-}2l)$ and the number of rectangles was represented by $N = \pi(R\text{-}2l)/A^{0.5}$, where R, l, and A are the diameter of a liposome, the height of a lipid, and occupied area for each lipid

molecule, respectively. Consequently, d was calculated by: $d = \pi R/N\text{-}A^{0.5}$. The estimated value of d was plotted against R (Fig. 4*c*), which showed that d was inversely proportional to R. The dependence of d on the diameter of liposomes was consistent with that of the ANS fluorescence of DOPC liposomes with a liner relationship between the ANS fluorescence and d, thereby arguing the critical role of membrane curvature (Fig. 4*d*). Importantly, the lag time of amyloid fibrillation showed a linear relationship with d, which indicated that membrane curvature and consequently water-accessible hydrophobic surfaces were critical for determining the lag time. (Fig. 4*e*).

On the other hand, the fluorescence of ANS increased in the presence of 2 μM Aβ (1-40) fibrils, with a slight blue shift being observed in the maximum to 510 nm (Fig. 4*a*). Thus, the fluorescence of ANS may also be useful for monitoring conformational changes in Aβ (1-40) as well as those of lipids. A further blue shift in the fluorescence of ANS to 480 nm occurred following the addition of 30 nm liposomes at 2 μM and this was accompanied by an increase in the intensity of fluorescence. The subtracted fluorescence spectrum suggested that the binding of Aβ (1-40) fibrils to membranes led to the additional binding of ANS (or a more hydrophobic environment on the pre-bound ANS molecules). The extent of the blue shift and increase in fluorescence intensity were less, following the addition of 100 nm liposomes at 2

μM, suggesting that additional ANS binding may be less for larger liposomes.

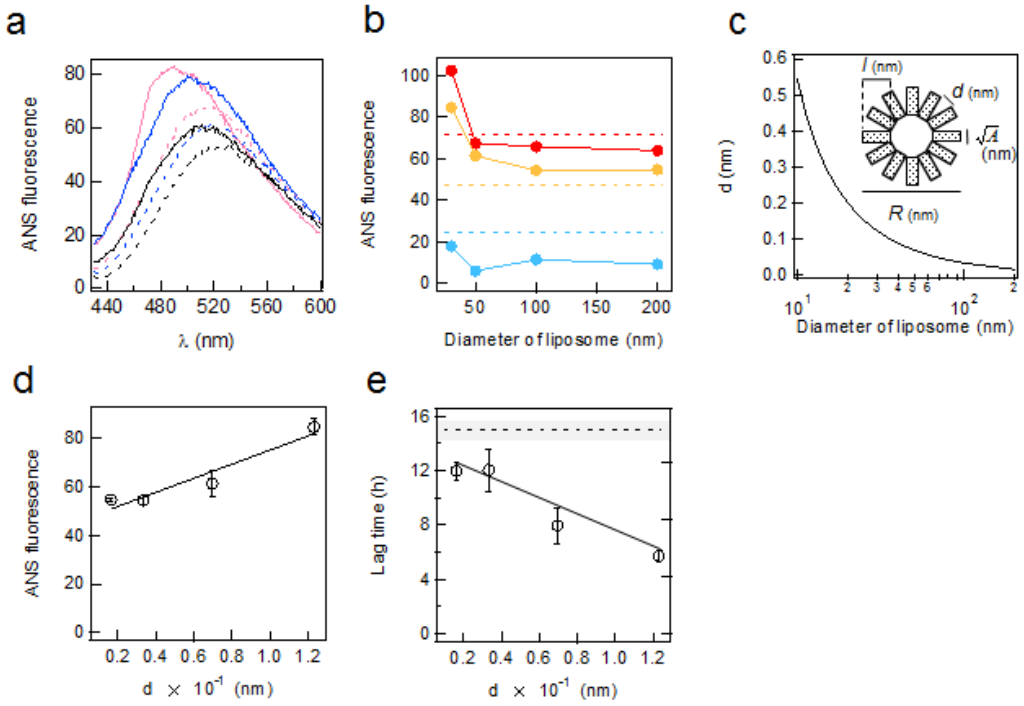

FIGURE 4. Exposed hydrophobicity of liposomes and its effects on the fibrillation of Aβ. (*a*) Fluorescence spectra of 2 μM ANS in the absence and presence of 2 μM DOPC liposomes and 2 μM Aβ fibrils. Black dotted line: ANS alone. Black solid line: Aβ fibrils. Blue dotted line: liposomes of 200 nm in diameter. Blue solid line: Aβ fibrils and DOPC liposomes of 200 nm in diameter. Magenta dotted line: liposomes of 30 nm in diameter. Magenta solid line: Aβ fibrils and liposomes of 30 nm in diameter. (*b*) ANS fluorescence (20 μM) at the maximal wavelength in the presence of 2 μM liposomes at various diameters in the presence (red) and absence (orange) of 2 μM Aβ fibrils. Blue circles indicate the difference between the presence and absence of Aβ fibrils. (*c*) The relationship between the distance, *d*, between two head groups of lipids and the diameter of DOPC liposomes. (*d*,

e) Dependencies of ANS fluorescence at 500 nm (*d*) and lag time (*e*) on *d*. Dashed lines indicate the ANS fluorescence (*b*) or lag time (*e*) in the absence of liposomes. The error bars indicate the standard deviation among three experiments. All experiments are conducted at 37 °C.

Fibril morphology

I examined the morphologies of fibrils prepared in the presence of DOPC liposomes with various diameters using TIRFM, AFM, and TEM (Fig. 5). I used liposomes in which rhodamine-labeled lipids were included for TIRFM so that I could also monitor the location of the liposomes. Liposomes were deformed by interaction with surfaces; therefore, the exact morphology of liposomes could not be detected by my measurements. The three methodologies covered a wide range of dimensions from nm to μm.

In the absence of liposomes, Aβ (1-40) fibrils were straight with a length up to several μM. They were well dispersed without clustering. Fibrils were still long and dispersed in the presence of 30 or 50 nm liposomes, although some clusters and fibril clumps were observed. In the TIRFM images, the locations of liposomes revealed by rhodamine fluorescence always overlapped with amyloid fibrils, which indicated that the liposomes were the sites of amyloid nucleation. The sizes of liposomes were markedly smaller than those of the fibrils.

AFM images indicated that fibrils became shorter and amorphous aggregates accumulated, with an increase in the size of liposomes, as was evident from AFM images obtained in the presence of 100 and 200 nm liposomes. TEM images in the presence of 100 and 200 nm liposomes revealed that fibrils associated with the ruptured liposomes. TIRFM

images in the presence of 100 and 200 nm liposomes showed the significant clustering of fibrils. TEM images in the presence of large liposomes showed thick and short fibrils. Taken together, the morphologies of Aβ (1-40) fibrils observed by TIRFM, AFM, and TEM depended on the size of the coexisting liposomes, which indicated that fibrils became shorter and clustered with an increase in the size of the liposomes and the amount of amorphous aggregates increased.

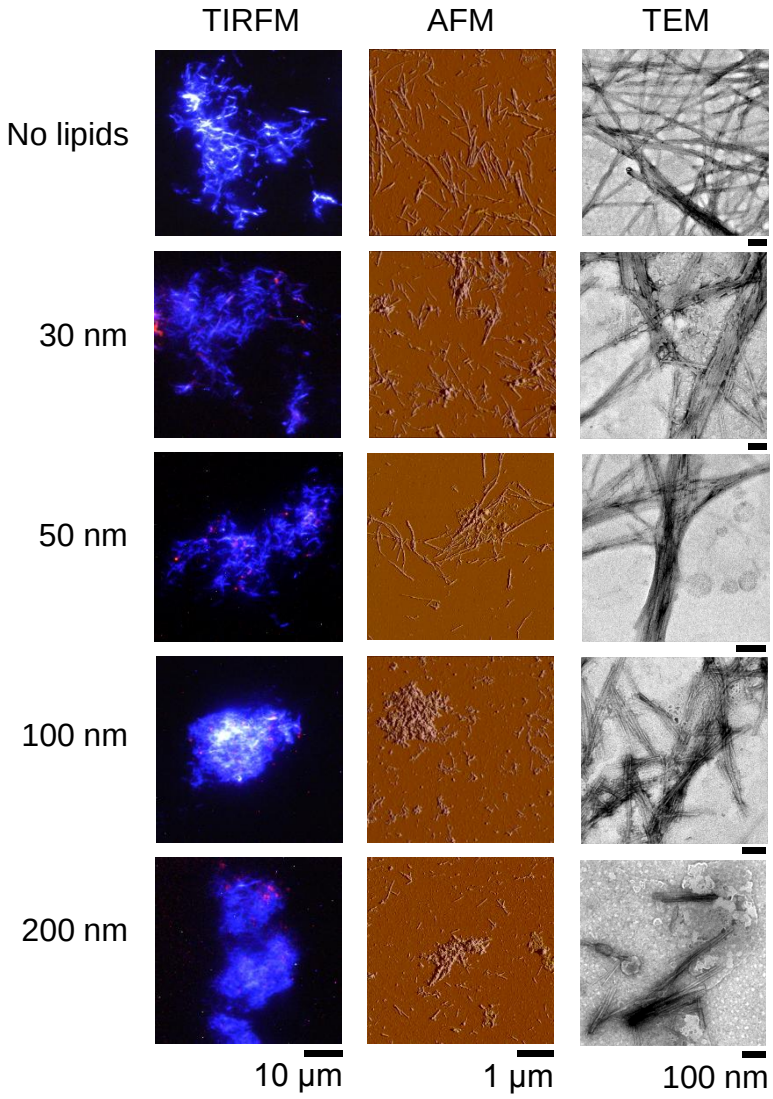

FIGURE 5. TIRFM, AFM, and TEM images of fibrils under DOPC liposomes of various sizes. The concentrations of Aβ and liposomes were 10 μM. In TIRFM images, fibrils and liposomes were monitored separately by ThT (blue) and Rhodamine (red), respectively. The scale bars of TIRFM, AFM, and TEM are 10 μm, 1 μm, and 100 nm, respectively.

Binding of Aβ (1-40) to liposomes characterized by ITC

In order to examine the interactions between Aβ (1-40) and DOPC liposomes, I performed ITC measurements (Fig. 6). Liposomes with the sizes of 30 nm and 100 nm were chosen to address the effects of high and low curvatures, respectively, on Aβ (1-40) fibrillation. Consecutive titrations of Aβ (1-40) to 30 nm liposomes in the ITC cell showed the positive ITC peaks with gradual decreases in the intensity (Fig. 6*a*). The heats of dilution and mixing of Aβ (1-40) to buffer were much smaller than those of Aβ (1-40) titrations to liposomes (Fig. 6*a*, inset). Thus, endothermic reactions indicated intermolecular interactions between Aβ (1-40) and 30 nm liposomes.

On the other hand, ITC thermogram of Aβ (1-40) titrations to 100 nm liposomes showed exothermic peaks which decreased gradually in amplitude (Fig. 6*b*). The extents of heat were larger than those observed when Aβ (1-40) was titrated to 30 nm liposomes (Fig. 6*a*). These data suggested that, although Aβ (1-40) was bound to both of 30 and 100 nm liposomes, the detailed mechanisms were distinct.

To obtain further insights into interactions between Aβ (1-40) and liposomes, I evaluated apparent thermodynamic parameters based on analyses of binding isotherms. The values of ${}^{app}K_d$ of Aβ (1-40) for 30 nm and 100 nm liposomes were 67.1 μM and 36.4 μM,

respectively. These values were smaller than those of α-synuclein binding to the liposomes (~30 nm) which mimicked presynaptic membranes ($^{app}K_d$ = 261 μM) or the liposomes which consisted of 1-palmitoyl-2-oleoyl-*sn*-glycero-3-phospho-(1′-*rac*-glycerol) ($^{app}K_d$ = 93 μM) (28). Accordingly, $^{app}\Delta G_{bind}$ (-6.3 kcal/mol) of Aβ to 100 nm liposome was smaller than that of Aβ to 30 nm liposome (-5.9 kcal/mol). These indicated that apparent binding affinity of Aβ (1-40) to DOPC liposomes was slightly stronger than those of α-synuclein to model liposomes and that affinity of Aβ to 100 nm liposome was slightly stronger than that to 30 nm liposome.

Interestingly, the sign and amplitude of $^{app}\Delta H_{bind}$ and $^{app}\Delta S_{bind}$ were different depending on the size of liposomes. The Aβ-30 nm liposome binding was driven by the positive entropy change ($T^{app}\Delta S_{bind}$ = 14.3 kcal/mol) to overcome the unfavorable endothermic reaction ($^{app}\Delta H_{bind}$ = 8.4 kcal/mol). On the contrary, the Aβ-100 nm liposome binding was favored by the negative enthalpy change ($^{app}\Delta H_{bind}$ = -62.0 kcal/mol) to overcome the entropy loss (T $^{app}\Delta S_{bind}$ = -55.7 kcal/mol). The large value of $^{app}\Delta H_{bind}$ in the Aβ-100 nm liposome binding may imply the complex mechanism in comparison with the Aβ-30 nm liposome binding. Similar complicated ITC results were observed for the α-synuclein binding to liposomes consist of 1,2-dioleoyl-*sn*-glycero-3-phospho-(1′-*rac*-glycerol) (73).

Moreover, biphasic patterns of each ITC peak in titration of Aβ to 100 nm liposomes suggested apparent two processes: the fast process with a sharp and intense peak was followed by the slow process with a broad and low intensity peak (Fig. 6*b*). These indicated that binding of Aβ to 100 nm liposomes was not a simple intermolecular interaction, although further studies are required to clarify the details of the liposome size-dependent binding of Aβ.

As can be seen in the ITC thermograms (Fig. 6), the binding reactions between Aβ (1-40) and liposomes did not saturate, which brought uncertainty of the fitting. Thus, the error values of K_a were large. Calculation of other thermodynamic parameters by using K_a with the large error further increased uncertainty. In order to obtain a saturated curve which can decrease errors, it was required to increase the concentrations of Aβ (1-40) in the syringe. However, the concentration of Aβ (1-40) (100 μM) used was already high and it was not practical to further increase the Aβ (1-40) concentration due to the formation of nonspecific aggregations. Although decreasing temperature to delay nonspecific aggregation might be an alternative possibility at higher Aβ (1-40) concentrations, there were concerns about changing the binding mode and/or aggregation pathway compared to those at 37 °C. Thus, I conclude that, although the errors were large, the ITC results clearly showed the distinct

bindings of Aβ (1-40) to the two kinds of liposomes and suggested that the binding mode and aggregation pathway of Aβ (1-40) depend on the degree of membrane curvature.

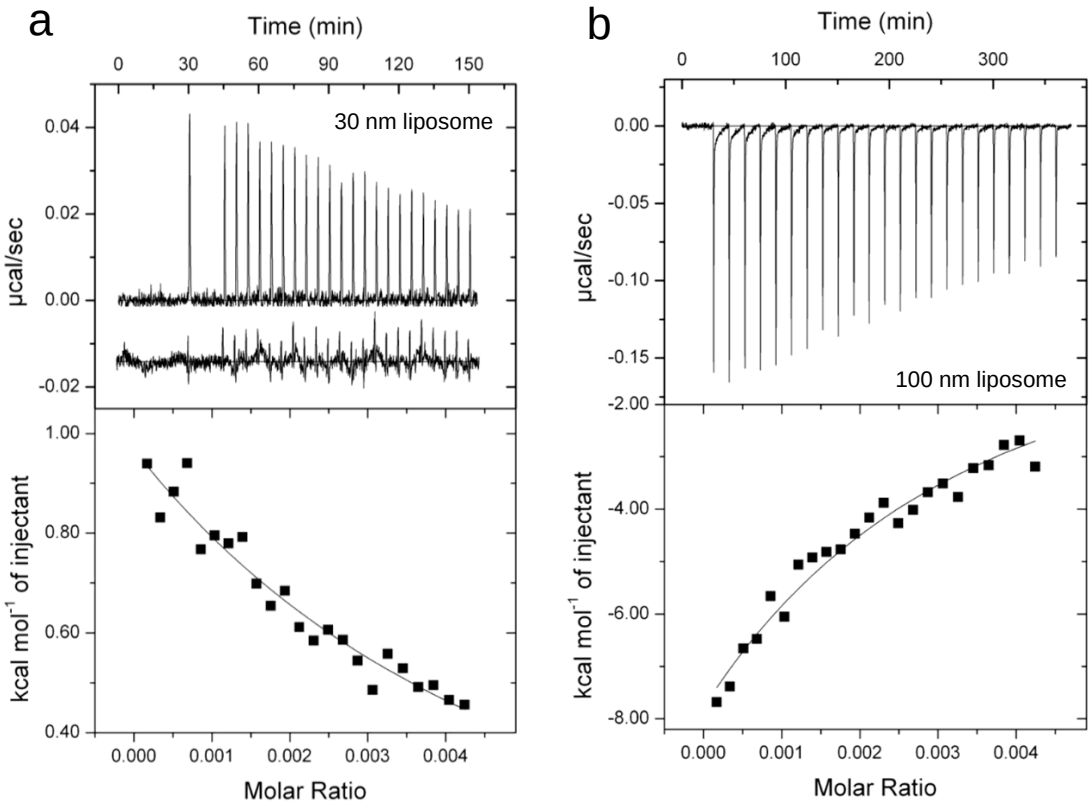

FIGURE 6. Isothermal titration calorimetry of DOPC liposomes with Aβ (1-40). (*a*, *b*) ITC thermograms (upper panel) and binding isotherms (lower panel) on titrating 30 nm (*a*) or 100 nm (*b*) liposomes with Aβ (1-40) are shown. ITC thermograms were obtained after the baseline correction. The spacing time between the first and second titrations was 900 s in *A*. The inset in *A* below the thermogram of Aβ titration indicates the small endothermic heat of dilution and mixing on Aβ (1-40) to buffer. The same scale of heat was used for comparison. The concentrations of liposomes were expressed by the molar ratio in binding isotherms those of lipid monomers based on the study by Otzen and coworkers (73). The solid lines in lower panels indicate the fitted curves.

Effects of anionic phospholipids on the fibrillation

In order to address the role of electrostatic interactions between Aβ (1-40) and membranes in fibrillation, I examined the effects of liposomes composed of DOPC and DOPS at a ratio of DOPC:DOPS = 1:1 (i.e. 50% DOPS liposomes). DOPS is one of anionic phospholipids reported to accelerate fibrillation of Aβ (1-40) and it has been suggested that phosphatidyl serine (PS) groups of DOPS liposomes interact with positive-charged Lys residue at the C-terminus of Aβ (1-40) (59). However, the dependence on the size of liposomes has not been examined. I monitored the fibrillation Aβ (1-40) in the presence of 50% DOPS liposomes of various sizes (Fig.7*a*). Only the 30 nm liposomes with 50% DOPS shortened the lag time (Fig.7*b*).

I then prepared the 30 nm liposomes composed of 100% DOPC, 50% DOPC and 50% DOPS, or 100% DOPS and monitored the fibrillation of Aβ (1-40) in the presence of these liposomes (Fig.7*c*, *d*). The liposomes containing 50% DOPS promoted the nucleation reaction as well as 100% DOPC liposomes. However, the degree of promotion of DOPS liposomes was small.

Thus, although the DOPS liposomes were reported to accelerate the Aβ (1-40) fibrillation (59), I saw no clear acceleration under the conditions. On the contrary, I observed

slightly adverse effects to suppress the accelerating effects produced by small DOPC liposomes. It is possible that, under my experimental conditions, the electrostatic interaction between negative-charged head group of PS and positive-charged amino acid residues of Aβ (1-40) tightly trapped the Aβ (1-40) molecules on liposomes so that further nucleation became difficult.

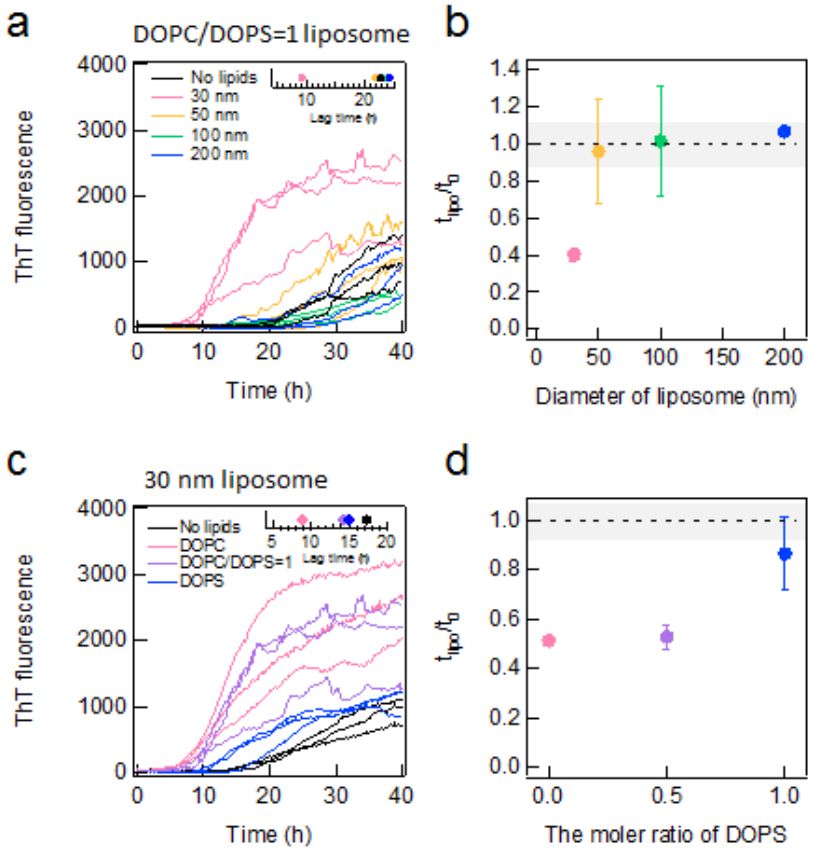

FIGURE 7. Effects of DOPS on the DOPC-dependent fibrillation of Aβ (1-40). (*a*, *b*) The kinetics of Aβ (1-40) fibrillation in the presence of 50% DOPS liposomes of 30 (pink), 50 (yellow), 100 (green), or 200 (blue) nm in diameter or without lipids (black) (*a*) and the dependence of relative lag time on the liposome size (*b*). The inset in *A* represents the average lag time at various liposome sizes. (*c*, *d*) The kinetics of Aβ(1-40) in the presence of 100% DOPC (pink), 50% DOPS (purple), and 100% DOPS (blue) liposomes of 30 nm in diameter (*c*) and the dependence of relative lag time on the DOPC content (*d*). The inset in *C* represents the average lag times at different contents of DOPS.

2-4. Discussion

I herein showed that DOPC liposomes markedly accelerated the fibrillation of Aβ (1-40), and that these effects depended on the size of liposomes even at the same total concentration of phospholipids: smaller liposomes more strongly accelerated fibrillation. Acceleration was suppressed by an increase in the liposome size. The amount of fibrils decreased and that of amorphous aggregates increased.

To understand these distinct effects of liposomes on fibrillation, I assumed two types of interactions between Aβ (1-40) and liposomes; one was productive binding leading to nucleation and fibrillation and the other was non-productive binding that formed amorphous aggregates (Fig. 8*a, b*). An analysis of the water-accessible hydrophobicity of liposomes probed by ANS binding and estimation of curvature suggested that small liposomes with higher surface curvature had more water-accessible hydrophobic regions and were effective for producing amyloid nucleation. Small liposomes with larger water-accessible hydrophobic regions interact with Aβ monomers weakly, concentrate them adequately to initiate nucleation. Although the binding of Aβ (1-40) to larger liposomes could also occur, it may be non-productive for amyloid nucleation because the local concentration was not sufficiently high to break supersaturation. Alternatively, although the local concentration was high, bound Aβ (1-40) molecules were tightly trapped on the surface of membranes and, thus, were

unable to diffuse and transform to seed competent conformations. The ITC measurements showed that affinity of Aβ to 100 nm liposome was slightly stronger than that to 30 nm liposome, consistent with the tighter binding and trapping of the Aβ (1-40) on the larger liposomes. These two types of interactions may propagate beyond liposome surfaces, leading to amyloid fibrillation or amorphous aggregation in bulk solvent.

The competitive mechanism between productive and non-productive binding (Fig. 8*a*) was analogous to the competition between amyloid fibrillation and amorphous aggregation in the absence of liposomes, as represented by a phase diagram of amyloid fibrillation dependent on salt and protein concentrations. Amyloid fibrils have been shown to form in the supersaturated solutions of responsible proteins via a nucleation and growth mechanism (63,74-76). Supersaturated regions can be classified into two types depending on the stability of supersaturation (Fig. 8*c*) (63). Supersaturation was remarkably stable in the metastable region, at which the solute concentration was slightly above the solubility, and seeding was essential to break supersaturation and make fibrils. Spontaneous fibrillation could occur after a certain lag time in the labile region, in which the driving force of precipitation increased. Various kinds of agitations such as shaking (77), stirring (78), or ultrasonic irradiation (31,32,66) have been shown to effectively force spontaneous fibrillation under these

supersaturated regions. One possible mechanism responsible for agitation-induced fibrillation is the concentration of amyloidogenic proteins at the hydrophobic air-water interface produced by agitation (63,79). Ultrasonication is known to produce cavitation bubbles with hydrophobic surfaces, and stirring or shaking will also increase the hydrophobic air-water interface. The hydrophobic air-water interface adsorbs proteins, concentrates them, and produces various aggregates including seed competent aggregates. Once amyloid fibrillation starts on the seeds, it even propagates to bulk regions without a hydrophobic surface.

Water-accessible hydrophobic surfaces produced by membrane curvature may play a similar role in membrane-assisted amyloid fibrillation to the air-water hydrophobic surface of cavitation bubbles induced by ultrasonic irradiation. Aβ monomers may be concentrated effectively by absorption to the hydrophobic surface due to membrane curvature. Thus, the membrane-assisted acceleration of fibrillation might be similar to the agitation-induced acceleration of fibrillation in the labile region (Fig. 8).

In the phase diagram, excessively strong precipitation forces produced glassy amorphous aggregates in which molecules were trapped in non-amyloidogenic conformations.

One possible mechanism underlying aggregation is that promiscuous interactions

between molecules produce various conformational states. In a similar way, various types of interactions on the membrane may trap the monomers preventing rearrangements to seed-competent conformations. The evenly dispersed charged head groups of phospholipids may contribute to preventing the bound Aβ monomers form associating to the seed-competent conformation. Thus, I considered that membrane-assisted amorphous aggregation corresponded to amorphous aggregation under strong forces of precipitation (Fig. 8).

Ban *et al.* (80) previously reported the amyloid fibrillation of Aβ (1-40) in real time at a single fibrillar level at pH 7.0 with TIRFM combined with the use of ThT. They used the surfaces of various chemically modified substrates. Extensive fibrillation was generally observed on surfaces with negative charges. In contrast, fibril growth was largely suppressed on positively charged or hydrophobic surfaces. A previous study reported that Aβ fibrillation was facilitated by negatively charged acidic phospholipids rather than neutral phospholipids (81). Because the pI value of Aβ is approximately 5, the net charge was slightly negative under neutral pH conditions. These results indicated that strong electrostatic attraction tightly trapped the Aβ (1-40) monomers on the surface so that subsequent lateral movement and nucleation were inhibited. The inhibitory role of a strongly hydrophobic surface can be also

explained in a similar manner assuming that the hydrophobic surface interacts with the hydrophobic residues of Aβ (1-40). These results support the view that there are two types of membrane binding, one leading to amyloid fibrillation and the other to amorphous aggregation.

Finally, although lipid rafts have been considered to play an important role in Aβ fibrillation (13,39-42), the underlying mechanism remains unclear (44,45). It is possible that the lipid raft carries the site of productive binding as proposed here more than the other lipid membranes. My proposal that there are two types of membrane binding for amyloidogenic proteins, one leading to amyloid nucleation and the other to non-productive binding and amorphous trapping, may be common for various amyloidogenic proteins. The specific removal of amyloidogenic proteins may be possible by preparing liposomes with only non-productive binding.

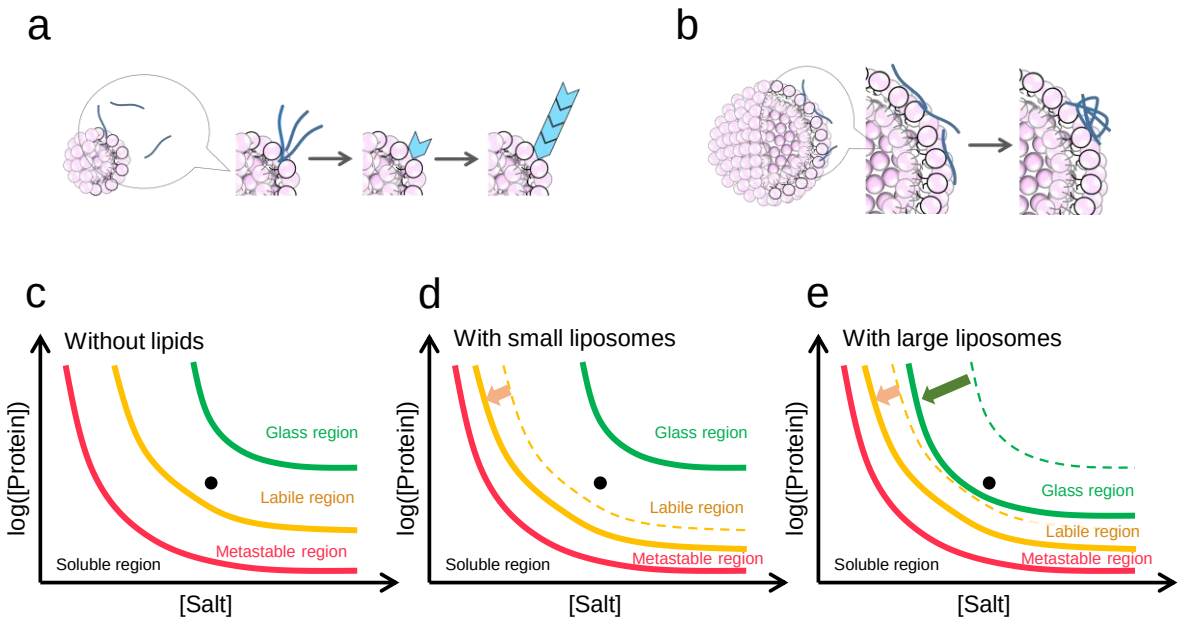

FIGURE 8. Schematic models of amyloid nucleation and amorphous aggregation on the surface of liposome membranes. (*a*-*b*) Schematic mechanism of the Aβ (1-40) fibrillation in the presence of liposomes. In the presence of smaller liposomes, Aβ (1-40) interacts with the surface of membrane weakly and this weak interaction promotes the nucleation. Aβ (1-40) is easy to remove due to this interaction and the elongation reaction is similar to without lipids (*a*). In the presence of larger liposomes, Aβ (1-40) interacts with the surface of membrane more strongly than that of smaller liposomes. This stronger interaction makes it difficult to induce nucleation and leads some Aβ peptides to amorphous aggregates. Other Aβ peptides

exist in medium and they form amyloid fibrils or amorphous aggregates (*b*). (*c*-*e*) Schematic phase diagram of conformational states of Aβ (1-40) in the absence (*c*) or presence of small (*d*) or large vesicles (*e*). The locations of the protein solutions as studied here are indicated by dots.

Chapter 3. Study on the mechanism of amyloidogenesis of α-synuclein on presynaptic membrane mimics

3-1. Introduction

Parkinson's disease (PD) is one of the most deleterious neurological diseases. One of the main causes of PD has been suggested to be the deposition of amyloid fibrils of α-synuclein (αSN) in the Lewy bodies (82). αSN is an intrinsically disordered protein which does not take defined three-dimensional conformations under physiological conditions. It consists of 140 amino acids and can be largely categorized to three regions: amphipathic N-terminal region (1-60), hydrophobic non-amyloid β component (NAC) region (61-95), and predominantly negatively-charged C-terminal region (96-140) (24).

In vitro experiments have shown that the fibrillation of αSN was susceptible to experimental conditions such as pH, salt concentration, temperature, and the presence of other amyloidogenic proteins or metal ions (83-85). Meanwhile, structural and physicochemical aspects of αSN have indicated that the fibrillation of αSN was also related to the length of C-terminal region. It was suggested that the difference in the length of C-terminal region included effects of the electrostatic contribution based on the large number of acidic amino acid residues: 15 residues in total at neutral pH (86-88). Deletion of C-terminal residues promoted the formation of amyloid fibrils. Various αSN mutants including the three familial variants for PD (A30P, E46K, and A53T) showed changes in the

propensity of aggregation and kinetics of amyloid fibrillation (89-92). A53T αSN mutant, which was the first mutant identified in the familial PD, promoted the fibrillation of αSN (89).

On the other hand, *in vivo* studies showed that αSN was localized in presynaptic nerve terminals and localization of αSN might be involved in a normal physiological function of αSN such as fusion of presynaptic vesicles (93-95). Moreover, amyloid fibrillation of αSN and its aggregates including amyloid fibrils and oligomers have shown cytotoxicity of neuronal cells (96). Coaggregation of αSN with lipid molecules was also observed (97). It was shown that αSN was bound to synaptic vesicles (98). This conformational change was also confirmed *in vitro* in the presence of micelles of sodium dodecyl sulfate (SDS) or liposomes of various lipids such as 1-palmitoyl-2-oleoyl-*sn*-glycero-3-phosphocholine (POPC) (98-101). Small unilamellar vesicles (SUV) which mimicked the membranes of presynaptic vesicles by assembling 1,2-dioleoyl-*sn*-glycero-3-phosphoethanolamine (DOPE), and 1,2-dioleoyl-*sn*-glycero-3-phospho-L-serine (DOPS), and DOPC in a ratio of 5:3:2 (referred to hereafter as Mimic) (28,102). This α-helical structure achieved by binding-induced folding reactions was suggested to be very stable (30). In addition, helical states in mixtures of water and either alcohol or SDS at low concentration were suggested to

be on-pathway intermediates for the formation of amyloid fibrillation (103,104), though there has been no compelling evidence for this (105). Recently, Fusco and coworkers have reported that N-terminal and NAC regions of αSN adopted helical structures on binding to SUVs although the exact binding regions depending on the species of lipids are not examined (28). Galvagnion and coworkers performed pioneer work on the mechanisms of fibrillation on SUVs prepared from the phospholipid 1,2-dimyristoyl-sn-glycero-3-phospho-L-serine (DMPS) (106). They showed that the presence of SUVs increased the rate of amyloid formation of αSN although they did not consider physiological conditions such as the presence of salts and lipid components of presynaptic vesicles.

Amyloid fibrillation proceeds via two steps: nucleation which produces a lag time thereby being a rate-limiting step and elongation where monomers are incorporated to active ends of fibrils for the rapid fibril growth. In order to facilitate nucleation, various agitation such as stirring and shaking has been applied to spontaneous fibrillation of monomers. Previously, Ohhashi et al. and So et al. (31,32) obviously demonstrated that ultrasonication was an efficient tool for accelerating fibrillation of amyloidogenic proteins and revealing the hidden propensity of amyloidogenicity through the promotion of nucleation.

In the current study, therefore, considering the effective fibril formation and

biological relevance of αSN, I examined the mechanism of αSN fibrillation by using ultrasonication and two-types of SUVs at the various concentrations of lipids ranging from 0 to 5 mM: one is a Mimic SUV and the other is a DOPC SUV for control. I revealed dual effects of Mimic SUVs on amyloidogenesis of αSN, promotion and inhibition of the formation of amyloid fibrils depending on the total concentration of lipids. While the fibrillation of αSN was promoted at a low concentration of lipids for Mimic SUVs, at a high concentration of lipids, the fibrillation was inhibited. Regardless of lipid concentrations for DOPC SUVs, the fibrillation was not accelerated.

Interestingly, as the concentration of lipids of Mimic was increased, the initial conformation of αSN changed from disordered states to α-helix-rich states as monitored in CD spectroscopy. However, significant structural transitions to α-helix were not detected when DOPC was added. Solution-state NMR spectroscopy further revealed binding regions of αSN for each SUV.

In order to examine the mechanism of αSN fibrillation in terms of initial bound conformation of αSN to SUVs, I used four αSN mutants: a familial mutant of αSN (αSN_{A53T}), C-terminally truncated two mutants which C-terminal 27 (αSN_{103}) and 11 residues (αSN_{129}) were eliminated, and a C-terminal (130-140) charge-neutralized mutant (αSN_{NC}). Although

all of mutants did not show remarkable changes in the conformation and behavior of fibril formation with DOPC SUVs, a lipid concentration-dependent conformation transition from disorder to helical states and distinct trends of fibrillation on Mimic SUVs were observed.

On the basis of these findings, I suggested that initial conformation of αSN including charged states and length of αSN and concentrations of lipids were key to determine a pathway to amyloid formation.

3-2. Experimental procedures

***Materials*—**DOPC, 1,2-dioleoyl-*sn*-glycero-3-phospho-L-serine (DOPS), and 1,2-dioleoyl-*sn*-glycero-3-phosphoethanolamine (DOPE) were purchased from Avanti Polar Lipids Inc. (Alabaster, USA). Thioflavin T (ThT) was obtained from Wako Pure Chemical Industries Ltd. (Osaka, Japan). All other reagents were obtained from Nacalai Tesque (Kyoto, Japan).

***Expression of αSN*—**Non-labeled αSN was expressed in *Escherichia coli* BL21 (DE3) (Novagen, Madison, WI) and purified as described (107). Briefly, αSN in fractured cells with ultrasonication was precipitated by ammonium sulfate at 75% (v/v). After centrifugation and dialysis, the solution containing αSN was applied to a Resource-Q column (GE Healthcare, Waukesha, WI), and then further purified by a COSMOSIL Protein R column (Nacalai Tesque, Kyoto, Japan). The purity of the solution was confirmed to be more than 95% by SDS-PAGE and MALDI mass spectroscopy. ^{15}N labeled αSN was expressed in BL21 (DE3) in BL media as a 5 mL pre-culture. Next, pre-culture of M9 media of 120 mL was inoculated and cultured overnight. Main culture of M9 (880 mL) was inoculated. The way of purification of ^{15}N labeled αSN was same as described above. αSN mutants (αSN_{A53T}, αSN_{103}, αSN_{129}, and αSN_{NC}) were expressed and purified in Kawata and coworkers in Tottori

University.

Preparation of SUVs—The compositions of vesicles used in this paper were DOPC and DOPC:DOPE:DOPS = 2:5:3 (Mimic). SUVs were prepared as previously described (108). Briefly, lipids were stored in chloroform stock solutions. Each composition was prepared at 10 μmol or 25 μmol in a glass tube. Lipid films were prepared by drying the solution in a stream of dry nitrogen, followed by desiccation for at least 1 h to ensure removal of the organic solvent. Buffer solutions of 1 mL were added to the glass tube and vortexed to rehydrate the lipid films. After ten freeze-thaw cycles, lipid suspensions were sonicated for 10 min on ice (TOMY, Tokyo, Japan). Then, to remove any titanium particles, the vesicles dispersion was centrifuged for 5 min at 8,000 rpm at 25 °C (Hitachi, Tokyo, Japan).

Amyloid fibrillation and ThT fluorescence assay—αSN was first dissolved at 200 μM in 20 mM sodium phosphate buffer (pH 7.4) containing 0.1 M NaCl. To measure protein concentration, absorbance at 280 nm was used. The formation of αSN fibrils was examined at 50 μM αSN in 20 mM sodium phosphate buffer containing 5 μM ThT, 0.1 M NaCl, and lipids of DOPC or Mimic SUVs at a desired concentration (0, 0.5, 1, 2, 3, 4, and 5 mM). Sample solutions of 200 μL were applied to three wells of a 96-wells microplate (Greiner-Bio-One, Tokyo, Japan) and a seal was affixed (PowerSeal CRISTAl VIEW, Greiner-Bio-One, Tokyo,

Japan). The plate was placed on a water bath-type ultrasonic transmitter with a temperature controller (ELESTEIN SP070-PG-M, Elekon Sci., Chiba, Japan), which can apply repetitive ultrasonication pulses to samples from three directions (32). The frequency of the ultrasonic waves was 17–20 kHz and the power output was set to 350 W. The periods under ultrasonication and quiescence were set as 1 min and 9 min, respectively. Fibril formation at 37 °C was monitored by ThT fluorescence hourly for 24 h with a microplate reader (SH-9000, Corona Electric Co., Ibaragi, Japan). The fluorescence intensity of ThT at 490 nm was measured with an excitation wavelength of 450 nm. Measurements were conducted with the multipoint measurement mode, and fluorescence values at 9 points in each well were averaged. The intensity of ThT fluorescence in each condition was described as the average value in the fluorescence values of three wells.

CD measurements—Far-UV CD spectra were measured with a Jasco 820 CD spectrophotometer (JASCO Corp., Tokyo, Japan). The condition of buffer solution and the concentration of αSN and lipids were same as described above. Measurements were performed at 37 °C using a quartz cuvette with a 0.1 mm path length, and the results were expressed as mean residue ellipticity [θ].

NMR spectroscopy—αSN samples, which were uniformly labeled with ^{15}N, were

prepared using 20 mM sodium phosphate buffer (pH 7.4) containing 0.1 M NaCl and 10% D_2O for ^{1}H-^{15}N heteronuclear single quantum correlation (HSQC) measurements. All HSQC spectra of 0.1 mM ^{15}N-labeled αSN in the absence and presence of DOPC or Mimic lipids at 0, 2, 6, 10, and 20 mM at 15 °C in an AVANCE-III H/D 800 spectrometer equipped with a cryogenic probe (Bruker BioSpin, Rheinstetten, Germany). Data were processed by NMRPipe and analyzed by Sparky.

AFM measurements—AFM images were obtained using a Digital Instruments Nanoscope IIIa scanning microscope (Veeco, Santa. Barbara, CA). A 20 μl sample solution of 100 μM αSN without lipids or with 5 mM DOPS or Mimic lipids was spotted onto freshly cleaved mica and left on the surface for 1 min. The surface was washed four times with 20 μl water and then blown off with compressed air. The scanning tip was a Si microcantilever and the scan rate was 1.0 Hz. The average height of the fibrils was estimated based on the peak height values measured.

3-3. Result

The importance of initial conformational states of αSN for fibrillation

In order to examine the initial structures of wild-type αSN (αSN_{WT}) at various concentrations of DOPC and Mimic lipids, I performed the far-UV circler dichroism (CD) spectroscopy (Fig. 1*a*). The far-UV CD spectrum of αSN_{WT} showed no characteristic peak, which indicated largely disorder conformation. In the presence of DOPC lipids, although the slight increases in the CD intensity at around 220 nm were observed, the gradual increase in the concentration of DOPC lipids to 5 mM did not show drastic changes in the CD intensity, suggestive of minimal structural changes of αSN_{WT} to α-helix.

Kinetics of αSN_{WT} fibrillation in the absence of lipids under quiescent conditions was observed by ThT fluorescence every 1 h. No marked increases in ThT fluorescence were observed even after 50 h of incubation (Fig. 1*a*), which indicated no formation of amyloid fibrils. The addition of 0.5 and 5 mM DOPC and Mimic lipid in the absence of ultrasonication did not induce fibrillation after 50 h of incubation (Fig. 1*a*).

Kinetics of αSN_{WT} fibrillation in the presence of 0.5 mM DOPC lipids and ultrasonication was monitored with ThT fluorescence. Ultrasonic treatment was repeated with a cycle of 1-min ultrasonication and 9-min quiescence for 24 h. The time-dependent ThT

fluorescence showed the sigmoidal curves with a lag time of ~15 h, which were typically observed in the spontaneous fibrillation of amyloid proteins. The far-UV CD spectrum also showed a typical pattern of cross-β structures of amyloid fibrils. Accordingly, it was concluded that amyloid fibrils of αSN_{WT} were formed with 0.5 mM DOPC SUVs and sonication.

The increases in the concentration of DOPC lipids, 1, 2, 3, 4, and 5 mM, also showed sigmoidal increases in ThT fluorescence (Fig. 1*a*). The maximum intensity of ThT fluorescence and lag time did not depend on the concentration of DOPC (Fig. 2*a, c*). The final far-UV CD spectra also showed the cross-β structures although spectra at 4 and 5 mM DOPC were different from the other spectra to some extent (Fig.1*a*). AFM images clearly showed the presence of short fibrils formed in 5 mM DOPC lipids and the absence of amorphous aggregates.

Effects of Mimic vesicles on the formation of amyloid fibrils of αSN_{WT} were investigated. The initial structural states of αSN_{WT} significantly depended on the concentration of Mimic lipids (Fig.1*a*). The increase in the concentration of Mimic lipids increased CD intensities at around 210 and 220 nm, which indicated the conformational transition αSN_{WT} to α-helix-rich structures and was consistent with the previous studies (28).

The formation of amyloid fibrils was also dependent on the lipid concentration in an opposite way of increasing helix. At the low concentration of Mimic lipids (0.5-3 mM), the fibrillation was promoted with showing the shortened lag time and high ThT fluorescence intensity (Fig. 2*b*, *c*). The maximum intensity of ThT fluorescence showed decreases with increasing lipid concentrations from 1 to 3 mM. The CD spectra indicated typical profiles of amyloid fibrils (Fig. 1*a*). However, at higher concentrations of lipids, 4 and 5 mM, no marked increases in ThT fluorescence were detected (Figs. 1*a* and 2*b*). The CD spectra still indicated helical structures (Fig. 1*a*). There were no appreciable aggregates in the AFM image obtained in 5 mM Mimic lipid although few short fibrils were observed.

The effects of ultrasonication on SUVs were most likely to be minimal since the power of ultrasonication for fibrillation was weaker than that for the preparation of SUVs. All of measurements were simultaneously performed using a 96-well plate. Consequently, artifacts on the current findings are excluded. However, these results suggested that the binding modes between αSN_{WT} and vesicles played the key role in whether the fibrillation was promoted or inhibited.

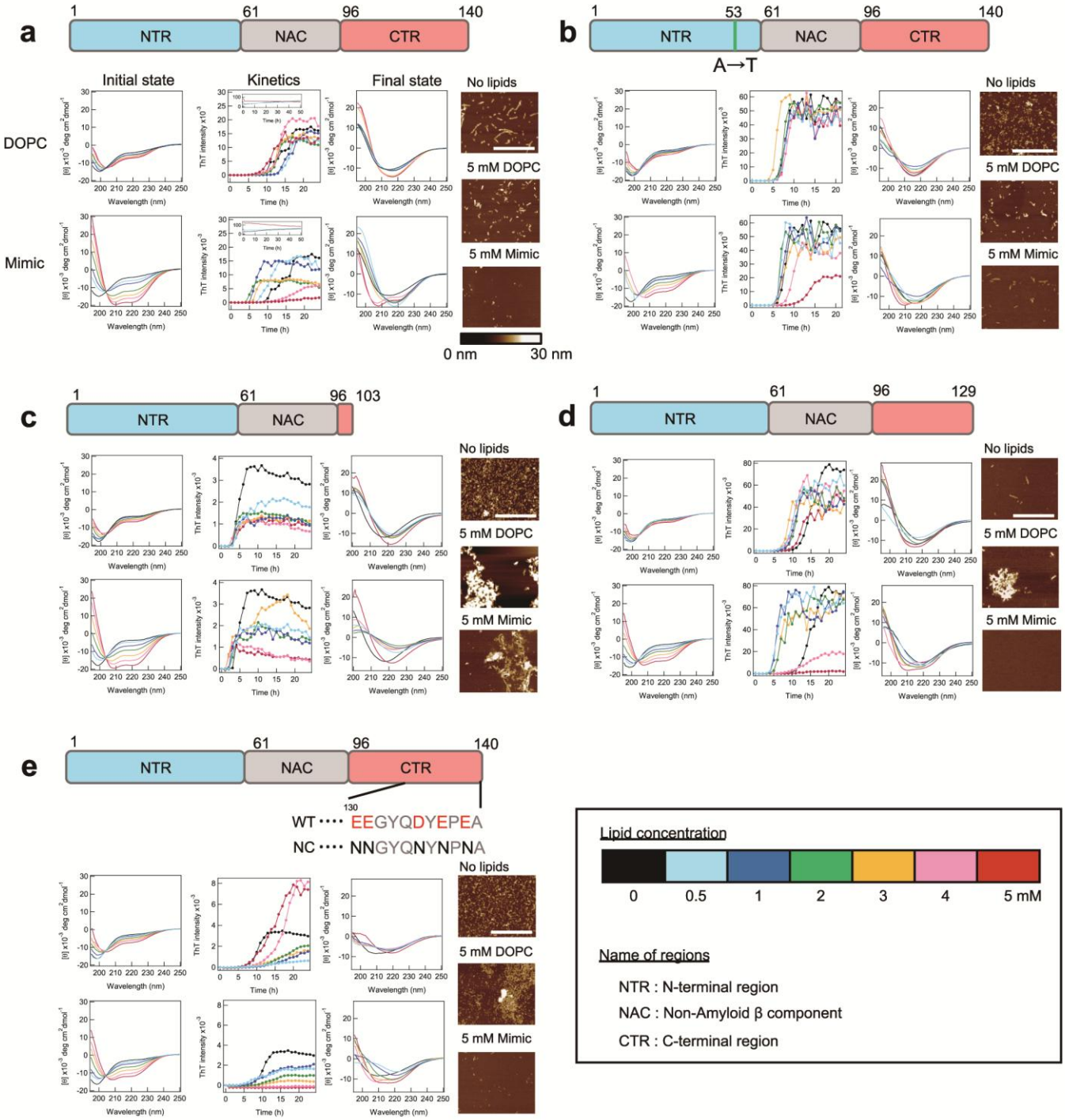
a
1
61
96
140
NTR
NAC
CTR
Initial state
Kinetics
Final state
No lipids
DOPC
5 mM DOPC
Mimic
5 mM Mimic
0 nm
30 nm
b
1
53
61
96
140
NTR
NAC
CTR
A→T
No lipids
5 mM DOPC
5 mM Mimic
c
1
61
96
103
NTR
NAC
No lipids
5 mM DOPC
5 mM Mimic
d
1
61
96
129
NTR
NAC
No lipids
5 mM DOPC
5 mM Mimic
e
1
61
96
140
NTR
NAC
CTR
130
WT ···· EEGYQDYEPEA
NC ···· NNGYQNYNPNA
No lipids
5 mM DOPC
5 mM Mimic
Lipid concentration
0
0.5
1
2
3
4
5 mM
Name of regions
NTR : N-terminal region
NAC : Non-Amyloid β component
CTR : C-terminal region

FIGURE 1. The conformational transition of αSN with distinct liposomes monitored by various methods. a-e) The far-UV CD spectra of wild-type αSN ($αSN_{WT}$) (a), a familial mutant of αSN ($αSN_{A53T}$) (b), C-terminally truncated two mutants which C-terminal 27 ($αSN_{103}$) (c) and 11 residues ($αSN_{129}$) (d) were deleted, and a C-terminal charge-neutralized mutant ($αSN_{NC}$) (e) were recorded immediately after the sample preparation (left panel) and incubation (right panel) in the presence of DOPC (upper panels) or Mimic SUVs (lower panels), respectively. Time dependent changes in ThT fluorescence at 485 nm were also monitored (middle panel). The insets in (a) show kinetics of fibrillation without lipids and with 5 mM DOPC and Mimic lipids without sonication. At the right, AFM images after reactions are shown without lipids and with 5 mM DOPC or Mimic. The scale bar represents 1 μm and the height of fibrils are shown below AFM images. Three major parts of αSN and mutated locations are schematically indicated with the residue number and color in the uppermost: N-terminal region (NTR) (blue), non-amyloid β component (NAC) (grey), and C-terminal region (CTR) (red). Distinct concentrations of lipids (DOPC or Mimic) were colored by black (0 mM), light blue (0.5 mM), blue (1 mM), green (2 mM), orange (3 mM), pink (4 mM), and red (5 mM) as indicated in the lower right.

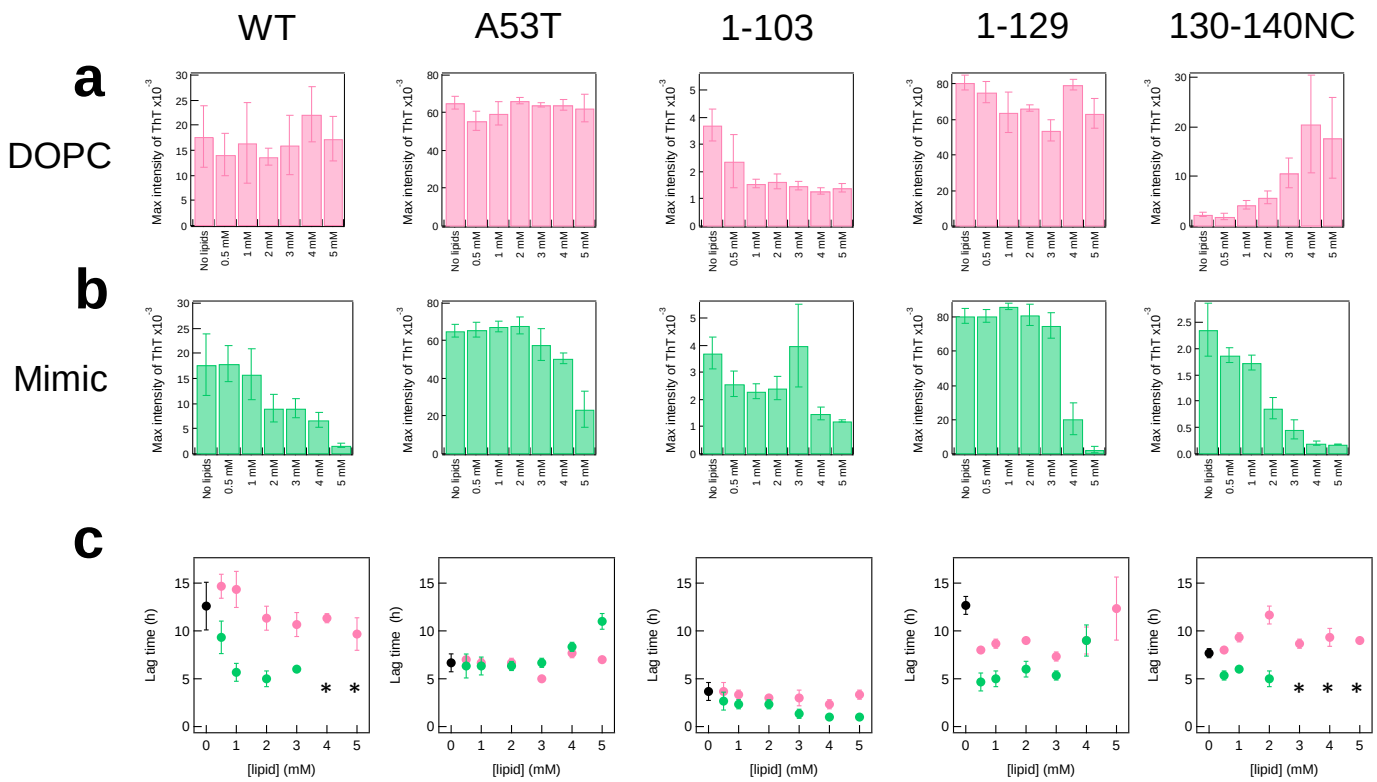

FIGURE 2. ThT fluorescence-based assay for amyloid formation at the various concentration of lipids. a-c) The maximum intensity of ThT fluorescence with lipids of DOPC (a) and Mimic SUVs (b) and lag time (c) for amyloid fibrillation of 5 kinds of αSNs were plotted against the concentration of lipids (0, 0.5, 1, 2, 3, 4, and 5 mM). The data of αSN_{WT}, αSN_{A53T}, αSN_{103}, αSN_{129}, and αSN_{NC} were displayed from the left. The lag times with DOPC or Mimic lipid and without lipids were indicated by red, green, and black circles, respectively. The data which did not provide reliable lag time due to low ThT fluorescence were indicated by asterisks. The average and error values were obtained from measurements in triplicate.

The effect of the difference in the binding between αSN and vesicles on the fibrillation

In order to obtain detailed insights into the importance of the binding modes in the fibrillation, I investigated the initial secondary structure and kinetics of fibrillation of A53T αSN mutant (αSN_{A53T}) in the presence of two-types of SUVs. This point mutation was one of familial PD mutants and was reported to change the binding mode of αSN to membranes since a hydrophobic residue of Ala was replaced to a hydrophilic Thr residue.

The far-UV CD spectrum of αSN_{A53T} without lipids showed a typical profile of unfolded proteins was almost similar to that of αSN_{WT} (Fig. 1*b*), which indicated that initial secondary conformations of αSN_{A53T} and αSN_{WT} were both identical. The addition of DOPC lipids changed CD spectra of αSN_{A53T} with the slight increases in CD intensity at around 220 nm. The changes in CD spectra of αSN_{A53T} were also very similar to those of αSN_{WT} and consistent with the previous study (109), suggesting that DOPC binding-induced conformational changes between αSN_{A53T} and αSN_{WT} were comparable.

The kinetics of αSN_{A53T} fibrillation in the presence of DOPC lipids was not different from that without DOPC (Fig. 1*b*). Thus, the lag times at the distinct concentration of lipid were all similar (Fig. 2*c*). The maximum intensity of ThT did not depend on the concentration of DOPC (Fig.2*a*). The CD spectra of αSN_{A53T} after incubation showed a

typical cross β-sheet structure of amyloid fibrils with a minimum around 215 nm (Fig. 1*b*). AFM images showed a number of short and thin fibrils without lipids and the absence of amorphous aggregates (Fig.1*b*). However, fibrils with 5 mM DOPC were thicker than those without lipids. The number of fibrils at 5 mM DOPC lipids appeared to be smaller than that without lipids. On the basis of the similar maximum intensity of ThT fluorescence and morphological differences in fibrils as shown in AFM images, the increase in the CD intensity with the increases in the concentration of lipid increased may be explained by polymorphic natures of amyloid fibrils.

Next, the initial secondary structures of αSN_{A53T} in the presence of Mimic lipids, the gradual addition of Mimic lipids increased the CD intensity at 220 nm as shown in αSN_{WT} (Fig. 1*b*), indicating the conformational transition to α-helix-rich structures. The kinetics of the formation of αSN_{A53T} amyloid fibrils was different from those of αSN_{WT} (Fig. 1*b*). The increase in ThT fluorescence of αSN_{A53T} was faster than that of αSN_{WT} (Figs. 1*a*, *b*). The lag time of αSN_{A53T} was shorter than αSN_{WT} (Fig. 2*c*), which agreed well with the previous study (89). The increases in the concentration of Mimic lipids changed ThT-based kinetics. At low and medium concentrations of lipids (0-2 or 3 mM), the kinetics and maximum intensity of ThT fluorescence were all similar (Figs. 1*b* and 2*b*) with similar lag

times of approximately 6 h (Fig. 2*c*), indicating no marked effects of Mimic lipids on the fibrillation. At higher concentrations of lipids over 3 mM, however, the slower kinetics with prolonged lag times by approximately 2 h (4 mM) ~ 5 h (5 mM) (Fig. 1*b*, 2*c*) and the decreases in the maximum intensity of ThT fluorescence (Fig. 1*b*, 2*b*) were observed.

The far-UV CD spectra of αSN_{A53T} samples below 3 mM Mimic lipid after incubation showed typical patterns of amyloid fibrils with a minimum intensity at around 215 nm (Fig. 1*b*). However, at 4 and 5 mM lipids, the far-UV CD spectra predominantly suggested not only cross-β but also α-helix conformations.

The AFM images at 0 and 5 mM DOPC lipids showed a number of fibrils (Fig. 1*b*). At 5 mM Mimic lipid, few fibrils were also detected and were thinner than those at 5 mM DOPC. All these results suggested the coexistence of molecular species of helical structures and fibrils at the high concentrations of Mimic lipids.

Residue-based NMR investigation on interacting residues of αSN with vesicles

In order to examine binding regions of αSN_{WT} for two-types of SUVs and conformational changes depending on the concentrations of component lipids, I performed the multi-dimensional NMR measurements of ^{15}N-labeled αSN_{WT}. The low temperature for ^{1}H-^{15}N HSQC measurements (15 °C) was used for obtaining more NMR cross peaks by minimizing the loss of peaks due to the fast hydrogen-deuterium exchange between amide protons and bulk protons.

The ^{1}H-^{15}N HSQC spectrum of αSN_{WT} in the absence of SUVs showed the narrow distribution of peaks centered at approximately 8.5 ppm with the intense peak intensity, which indicated largely unfolded conformations and was well consistent with other studies (Fig. 3*a*). In order to reveal residues responsible for binding with SUVs, titration of 2, 6, 10, 20 mM DOPC or Mimic lipids to 100 μM αSN_{WT} solutions was carried out. No changes in the chemical shifts were observed (Fig. 3*a*). Thus, I examined the changes in the peak intensity of αSN_{WT} in the absence and presence of lipids by taking advantage of local flexibility-dependent NMR peak intensity. Sharp peak intensity of αSN_{WT} will be lost beyond the detection level due to the severe peak broadening coming from the complex formation with large molecular sizes of SUVs. However, highly flexible residues which are not bound

to SUVs will retain the peak intensity by overcoming fast relaxation.

For the peak intensity analysis, the peak intensity without (I_0) and with lipids (I) was normalized by dividing intensity of each residue by the average intensity of 120-140 residues and compared by taking a ratio of I/I_0 (Fig. 3*b* and 4*b*). The addition of DOPC lipid of 2 mM did not change the ratio of I/I_0 (1±0.05) (Fig. 3*b*). As the concentration of DOPC was increased to 6, 10, and 20 mM, I/I_0 values of the N-terminal and NAC region slightly decreased (Fig. 3*b*). These results indicated the weak intermolecular interactions between αSN_{WT} and DOPC SUVs and the minimal conformational changes of αSN_{WT}.

More dynamic changes in I/I_0 were detected in the presence of Mimic lipids (Fig. 4). At 2 mM Mimic lipid, the I/I_0 value of the N-terminal and NAC region was roughly 0.7 and gradually increased along residue numbers (Fig. 4*b*). The profile of I/I_0 was very similar to that at 6 or 10 mM DOPC lipids. The more significant decreases in I/I_0 were observed when the concentration of Mimic lipids were increased to 6, 10, and 20 mM (Fig. 4*b*). I/I_0 values of the N-terminal and NAC regions at 6, 10, and 20 mM of Mimic lipids were roughly ~0.39, 0.32, and 0.06, respectively, and gradually increased along residue numbers (Fig. 4*b*).

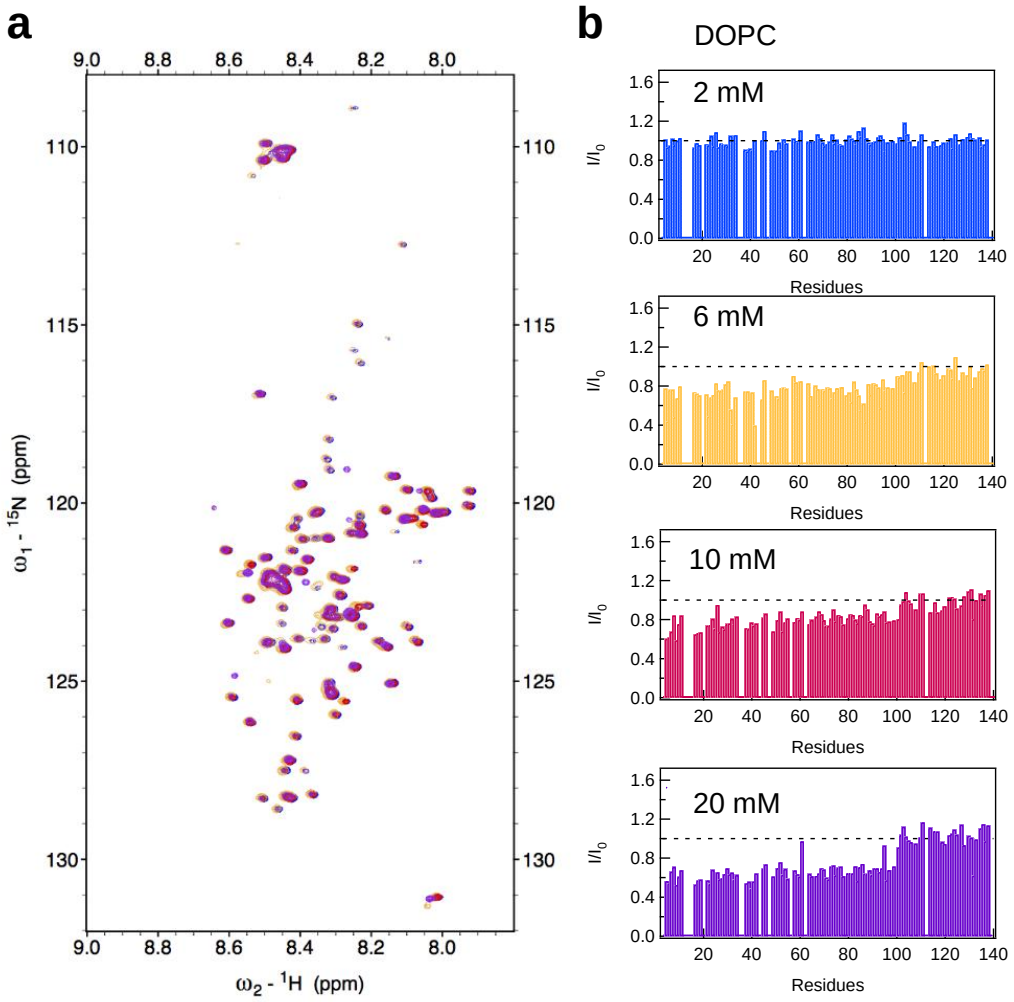

FIGURE 3. NMR spectroscopy of wild-type αSN and peak intensity analyses at the various concentration of DOPC lipids. a) The superposition of ^{1}H–^{15}N HSQC spectra of ^{15}N-labeled αSN at 2 (blue), 6 (orange), 10 (red), and 20 mM lipids (purple) of DOPC. b) The ratio of the peak intensity of αSN (I/I_0) with (I) and without (I_0) DOPC was plotted as a function of the residue number of αSN. The concentration of lipid used were shown in each panel. The data points in N-terminal region covering the C-terminal residual peaks were removed.

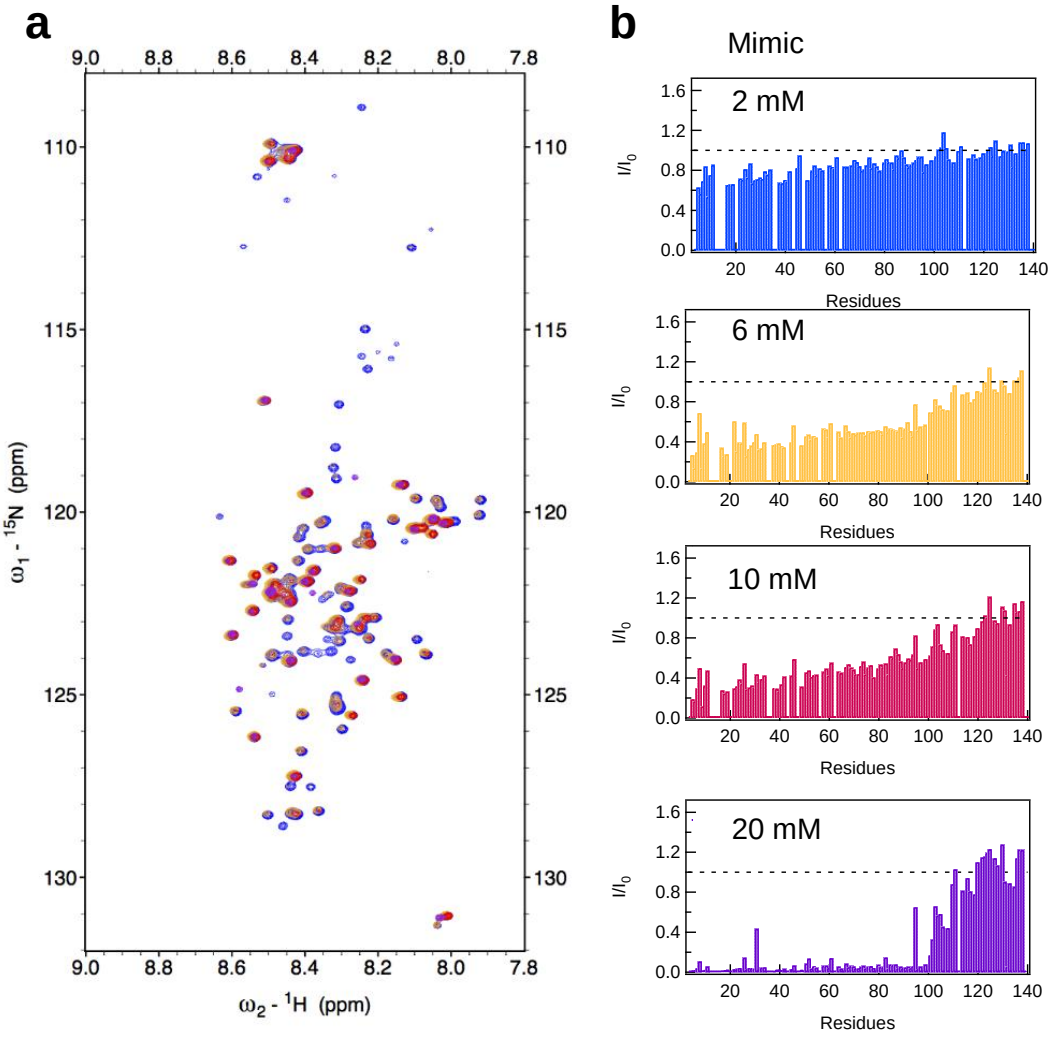

FIGURE 4. NMR spectroscopy of wild-type αSN and peak intensity analyses at the various concentration of Mimic lipids. a) The superposition of ^{1}H–^{15}N HSQC spectra of ^{15}N-labeled αSN at 2 (blue), 6 (orange), 10 (red), and 20 mM lipids (purple) of Mimic. b) The ratio of the peak intensity of αSN (I/I_0) with (I) and without (I_0) Mimic was plotted as a function of the residue number of αSN. The concentration of lipid used were shown in each panel. The data points in N-terminal region covering the C-terminal residual peaks were removed.

The effect of the C-terminal region of αSN on its amyloidogenesis

C-terminally-truncated αSN has shown to be accumulated in Lewy bodies and more rapid fibrillation than that of αSN_{WT}: however, the effects of vesicles on the fibril formation of C-terminally-truncated αSN mutants remain unclear. In order to investigate interactions between C-terminally-truncated αSN mutants and SUVs and their effects on fibrillation, I used the two αSN mutants which C-terminal 27 residues from 104 to 140 (αSN_{103}) and 11 residues from 130 to 140 (αSN_{129}) were truncated, respectively (87).

I first examined the formation of amyloid fibrils of αSN_{103} in the absence and presence of SUVs (Fig.1*c*). The initial secondary structure of αSN_{103} in the absence of SUVs was investigated by the far-UV CD spectroscopy. The far-UV CD spectrum showed a typical pattern of disordered proteins without a characteristic peak (Fig. 1*c*). The addition of DOPC lipids slightly increased the CD intensity of αSN_{103}. The faster increase in ThT fluorescence than that of αSN_{WT} was observed. The far-UV CD spectrum of αSN_{103} without lipids indicated the formation of fibrils with a minimum at ~218 nm (Fig. 1*c*). A number of fibrillar aggregates were detected in the AFM image.

Kinetics, monitored by ThT fluorescence, were not altered with DOPC lipids and did not depend on the concentration of lipids. The lag time was all around 3 h (Fig. 2*c*)

although the maximum intensity of ThT fluorescence was low compared to that in the absence of DOPC lipids (Fig.2*a*). The far-UV CD spectra in the presence of DOPC lipids after incubation suggested cross β-structures of amyloid fibrils with minimum at ~222 nm (Fig. 1*c*). The AFM image at 5 mM DOPC lipids showed that the clusters of amyloid fibrils. The sticky propensity of fibrils at 5 mM DOPC lipids may be involved in the decreases in ThT fluorescence compared to that without DOPC lipid.

As observed in full-length αSN, Mimic lipids increased the CD intensity of the initial structure at 210 and 220 nm (Fig. 1*c*), which indicated the induction of α-helical structures in a concentration-dependent manner (Fig.1*d*). ThT-based monitoring of amyloid fibrillation at the various concentrations of Mimic lipids showed the increases in ThT fluorescence after a lag phase. As the concentration of Mimic lipids increased, the lag time was shortened from ~3 to ~1 h (Fig. 2*c*) and the maximum intensity of ThT fluorescence mostly decreased except for data at 3 mM Mimic lipid (Fig. 2*a*).

The secondary structures of the final products were also examined using the far-UV CD spectroscopy. The CD spectra revealed the two-types of cross β structures of amyloid fibrils which showed a minimum at ~225 nm at 0-3 mM of Mimic lipids and at ~220 nm at 4 and 5 mM of Mimic lipids (Fig. 1*c*). The AFM image at 5 mM of Mimic lipids demonstrated

the formation of amyloid fibrils even at a higher concentration of Mimic lipids (Fig. 1*c*). All these results indicated the formation of amyloid fibrils at all the concentrations of Mimic lipids used. However, it should be mentioned that the low maximum intensity of ThT fluorescence and high CD intensity at the high concentration of Mimic lipids may be attributed to the polymorphic natures of amyloid fibrils.

Next, I investigated the conformational changes of αSN_{129} with SUVs and the formation of amyloid fibrils of αSN_{129} in the absence and presence of SUVs (Fig.1*d*). The initial secondary structure of αSN_{129} without SUVs was examined using the far-UV CD spectroscopy. The far-UV CD spectrum displayed a typical pattern of largely disordered proteins without a characteristic peak (Fig. 1*d*). The trace of ThT fluorescence for αSN_{129} without SUVs showed a sigmoidal curve of amyloid formation with a lag time of ~13 h and the far-UV CD spectrum showed the pattern of amyloid fibrils (Fig. 1*d*). The AFM image revealed the presence of short fibrils.

The increment of the DOPC concentration slightly increased the CD intensity of αSN_{129} as observed other αSNs. The kinetic experiments which monitored ThT fluorescence at the various concentration of DOPC lipids showed the promoted nucleation reaction with shortened lag times (7-8 h) without the concentration dependence of DOPC except for 5 mM

DOPC (Fig. 2*a*, *c*). The maximum intensity of ThT fluorescence was all high and also did not show the significant DOPC concentration dependence. At all of the concentration of DOPC lipids, the far-UV CD spectra after incubation of more than 20 h showed the cross β-structures of amyloid fibrils although the intensity and wavelength of minimum intensity more or less differed (Fig. 1*d*). The AFM image at 5 mM DOPC showed the clusters of fibrils as observed in that of αSN_{103} fibrils at the same DOPC concentration.

The addition of Mimic lipids showed drastic changes in conformation and aggregation behavior of αSN_{129}. With the increase in the concentration of Mimic lipids, the characteristic peaks at 210 and 220 nm in the far-UV CD spectra of the initial structures appeared and their CD intensities gradually increased (Fig. 1*d*), which indicated that the increase in the extent of α-helical structures.

Time-dependent monitoring of ThT fluorescence revealed the two distinct effects on kinetics of fibrillation of αSN_{129}: promotion of fibrillation at the low concentration of Mimic lipids ranging from 0.5 to 3 mM with a lag time of ~5 h and inhibition of fibrillation at the medium and high concentration (4 and 5 mM) with a lag time of ~9 h for 4 mM (Fig. 2). Even after a long incubation more than 20 h with ultrasonication, I could not observe the increase in ThT fluorescence at 5 mM Mimic lipid.

The maximum ThT intensity significantly decreased at 4 mM Mimic lipid and almost no ThT fluorescence was obtained at 5 mM (Fig. 2*b*). The far-UV CD spectra of αSN_{129} sample solutions after the reaction indicated the formation of β-sheet-rich structures at the low and medium concentrations of Mimic lipids, however, at the high concentrations of 4 and 5 mM, the spectra still showed the pattern of α-helical structures. In AFM image at 5 mM Mimic lipid, no appreciable fibrils and/or aggregates were observed. Considering all results of CD, ThT assay, and AFM images, the high concentration of Mimic lipids stabilized α-helical conformations of αSN_{129}. Finally, various results on αSN_{103} and αSN_{129} raised a strong possibility that the C-terminal region was responsible for amyloidogenicity of αSN.

The effect of charges in the C-terminal region on its amyloidogenesis

In order to clarify the contribution of negative charges in the C-terminal region of αSN to its conformational transition and amyloidogenicity on SUVs, I further used a charge-deleted full-length mutant of αSN in which four Glu residues and one Asp residue located between positions 130 and 140 were replaced by Asn residues (αSN_{NC}) (87).

The soluble monomers of αSN_{NC} in the absence of SUVs showed a far-UV CD spectrum of largely disordered proteins as observe in other αSNs used here (Fig. 1*e*). The real-time observation of ThT fluorescence showed the rapid increase in the intensity of ThT (Fig. 1*e*) with a lag time of 7 h (Fig. 2*c*). This result indicated the faster fibrillation of αSN_{NC} than that of αSN_{WT}, which was consistent of the previous study by Izawa and coworkers (87). The far-UV CD spectrum indicated the formation of amyloid fibrils. A number of fibrils were also observed in the AFM image (Fig. 1*e*).

The far-UV CD spectra at the various concentrations of DOPC lipids from 0 to 5 mM showed that the addition of DOPC changed the initial secondary structures of αSN_{NC} to more structured states with the increases in the CD intensity (Fig. 1*e*). The increases in the CD signals depended on the concentration of DOPC lipids. ThT assay showed a variety of kinetic traces of αSN_{NC} depending on the concentration of DOPC lipids. At the low and

medium concentration of DOPC lipids, the increases in ThT fluorescence appeared to be suppressed although the increases in the concentration of DOPC lipids to 2 and 3 mM recovered ThT fluorescence (Fig. 1*e*). The maximum intensity of ThT fluorescence increased with the increase in the lipid concentration (Fig. 2*a*). The CD spectra after the reactions showed cross β-structures of amyloid fibrils although the intensity of CD signals was low (Fig. 1*e*). In the AFM image at 5 mM DOPC lipid, a number of fibrillar aggregates were detected. Polymorphic property of amyloid fibrils or coexistence of other aggregates including cross β-structures-containing oligomers and amorphous aggregates may account for dynamic changes of results, e.g., the distinct kinetics, maximum intensity of ThT fluorescence, and CD spectra depending on the concentration of DOPC lipids.

In the presence of Mimic lipids, αSN_{NC} adopted α-helical structures with showing minima at 210 and 220 nm in a lipid concentration-dependent manner (Fig.1*e*). The kinetics of ThT fluorescence also depended on the concentrations of Mimic lipids (Fig.1*e* and 2*c*). The max intensity of ThT decreased as the concentration of Mimic lipids increased (Fig. 2*b*). At 0-3 mM of Mimic lipids, the kinetic profiles of αSN_{NC} showed a typical sigmoidal increase in ThT fluorescence of amyloid fibrillation. The lag time of nucleation was approximately 5 h (Fig. 2*c*). At the high concentration of Mimic lipids, 4, and 5 mM, no

appreciable increases in ThT fluorescence were observed even after an incubation of 24 h. The far UV-CD spectra at 0-3 mM lipid concentrations showed the patterns of β-sheet-rich structures, although that at 3 mM included α-helix structures. However, those at 4, and 5 mM indicated α-helix-rich structures (Fig. 1*e*). The AFM image at 5 mM Mimic lipid, any aggregates were not detected. Thus, αSN_{NC} formed fibrils at the low concentration of Mimic lipids, however, at the high concentration of lipids, αSN_{NC} did not form fibrils and maintained the initial structures of α-helix. Since the aggregation behaviors of αSN_{NC} were different from those of αSN_{WT}, negative charges in the C-terminal part of αSN affect its amyloidogenicity.

3-4. Discussion

This study clearly indicated that the initial structure of non-α-helical αSN was important for forming amyloid fibrils in the presence of SUVs. Thus, in order to correlate amyloidogenesis and α-helical conformations, I examined the content of α-helical structures and the other secondary structures of αSN at the various concentrations of DOPC or Mimic lipids using a software of BESTSEL (http://www.bestsel.elte.hu) (110). BESTSEL accurately predicted the content of the secondary structures of proteins and aggregates such as α-helix, β-sheet, and the other structures including random coils and turn structures, based on the CD spectrum (Fig. 5).

The predicted results showed that the amount of α-helix significantly increased as the concentration of Mimic lipids increased while the amount of the others decreased. The results clearly indicated a Mimic SUV-induced conformational transition to α-helix of αSN_{WT} at the high concentration of Mimic lipids, which inhibited the formation of amyloid fibrils. The full length familial mutant, αSN_{A53T}, showed the similar conformational change and fibrillation profiles, although the point mutation at Ala53 affected amyloidogenesis of αSN.

However, the correlation of helicity and amyloidogenicity disappeared with the deletion of the C-terminal region of αSN. αSN_{103} with the high content of α-helix at the high

concentration of Mimic lipids formed amyloid fibrils (Fig.1*c* and 5*c*). Interestingly, αSN_{129} showed the both properties of full-length αSNs and αSN_{103} (Fig. 1*d* and 5*d*). Meanwhile, a full-length charge-deleted mutant of αSN_{NC} recovered the aggregation pattern of αSN_{WT} although inhibitory effects appeared at the lower concentration of Mimic lipids than the other full-length αSNs (Fig. 1*e* and 5*e*). These findings suggested that the charged state and the length of unfolded region that was not bound to membranes were responsible for amyloidogenicity and should be also considered with α-helical structures.

Taken all together, I suggest the schematic models which describe the various pathways for the formation of amyloid fibrils of αSNs in the presence of Mimic vesicles at the distinct concentrations on the basis of the charged state and the length of unfolded region (Fig. 6).

αSN including more than half of the C-terminal region was dissolved in solutions (Fig. 6*a(i)*). At the low concentration of Mimic lipids when the ratio of proteins to vesicles is very high, full-length αSNs weakly interact with Mimic SUVs, (Fig. 6*a*(ii)). As the concentration of Mimic lipids increases, binding proteins/vesicles decreases and the extent of α-helix increases (Fig. 6*a(iii), (iv)*).

NMR data (Fig. 4) and the results of the initial secondary structure (Fig. 1*a*)

indicated that the parts of αSN binding to Mimic vesicles were similar between at 6 and 10 mM Mimic lipids, but the extent of α-helical structure was different. Therefore, it was suggested that the binding of αSN to the vesicles of Mimic and the conformational change to α-helical structure depended on the concentration of Mimic lipids (Fig. 6*a(iii), (iv)*). The conformational change due to the high concentration of Mimic vesicles and binding of α-SN to the vesicles might affect the fibrillation.

Therefore, the binding modes of full-length αSNs are different at each concentration of Mimic lipids. These differences may cause distinct kinetics of the fibrillation (Fig. 1and 5*a*). At the low and middle concentration of Mimic lipids, the formation of amyloid fibrils is promoted by an efficient nucleation through a weakly-bound αSNs and a lot of free αSNs (Fig. 6*a(v)*). However, at the high concentration of Mimic lipids, the fibrillation is inhibited due to the high stability of α-helical structures which hamper a conformational transition to cross β-sheet structures of amyloid fibrils. The high binding affinity of α-helical structures for Mimic SUVs decreases the number of free αSNs for nucleation.

On the other hand, the pathway of the formation of amyloid fibrils of C-terminal truncated mutants of αSNs, αSN_{103} and αSN_{129}, is discriminated from that of full-length αSNs (Fig. 6*b*). The deletion of the C-terminal region accelerates amyloid fibrillation due mainly to

the attenuation of the intermolecular electrostatic repulsion thereby enhancing an efficient nucleation and elongation of fibrils (Fig. 1*c*, *d*, and 4*b*). In addition, considering the small dependence of lipid compositions on kinetics of fibrillation of αSN_{103} and αSN_{129} (Fig. 1*c*, *d*, and 2), intermolecular hydrophobic interactions in the NAC region are key to nucleation (Fig. 1*c* and 6*b*).

Recently, it has been reported that the number of vesicles and αSN molecules in a functional synaptosome, which is an isolated synaptic terminal from a neuron, are ~400 and ~3000, respectively, i.e., the ratio of αSN to vesicles is ~10 (111). Galvagnion and coworkers have shown that lipid vesicles enhanced amyloid fibril formation when 1,2-dimyristoyl-*sn*-glycero-3-phospho-L-serine (DMPS) to αSN was below 40, which corresponded that the ratio of αSN to vesicles was 100 (106). In this study, when the ratio of Mimic lipids to αSN was below ~80, which corresponded that the ratio of αSN to vesicles was 50, amyloid fibril formation was enhanced.

The lipid composition and reaction buffer used in the current study was different from that used by Galvagnion and colleagues. The negative charge of the surface of Mimic SUVs decreased by ~30% compared with that of DMPS SUVs under the assumption that the number of lipid molecules per one SUV was same. So, it was reasonable that

proteins/vesicles ratio in this study was increased. It should be highlighted that our experimental conditions of the lipid composition and reaction buffer with the ionic strength were closer to physiological conditions than those of Galvagnion and coworkers. Therefore, I could reach a biologically and pathologically important conclusion: under normal concentrations of αSN in a synaptic terminal, the concentration of synaptic vesicles was sufficient enough to inhibit the formation of amyloid fibrils. However, the disruption of the balance of a ratio of αSN to vesicle by the failure of quality controls in cells may trigger to the formation of amyloid fibrils. As revealed in this study, mutation can also change this balanced ratio. Although the more compelling results are required, one of familial PD, αSN_{A53T}, and C-terminal truncated mutants, αSN_{103} and αSN_{129}, might be higher ratio of αSN to vesicle than that of αSN_{WT}, under the same concentration of Mimic lipids.

The fibrillation pathway of αSN is highly complicated in the presence of vesicles. However, this study proposed that the initial structure was important in the formation of amyloid fibrils, binding modes of αSN to SUVs depended on the concentration of vesicle lipids, and the charge state and length of C-terminal region affected the fibrillation. I expect that the current findings and suggestions can provide insights into understanding of the mechanism of amyloidogenesis of αSN in a synaptic terminal.

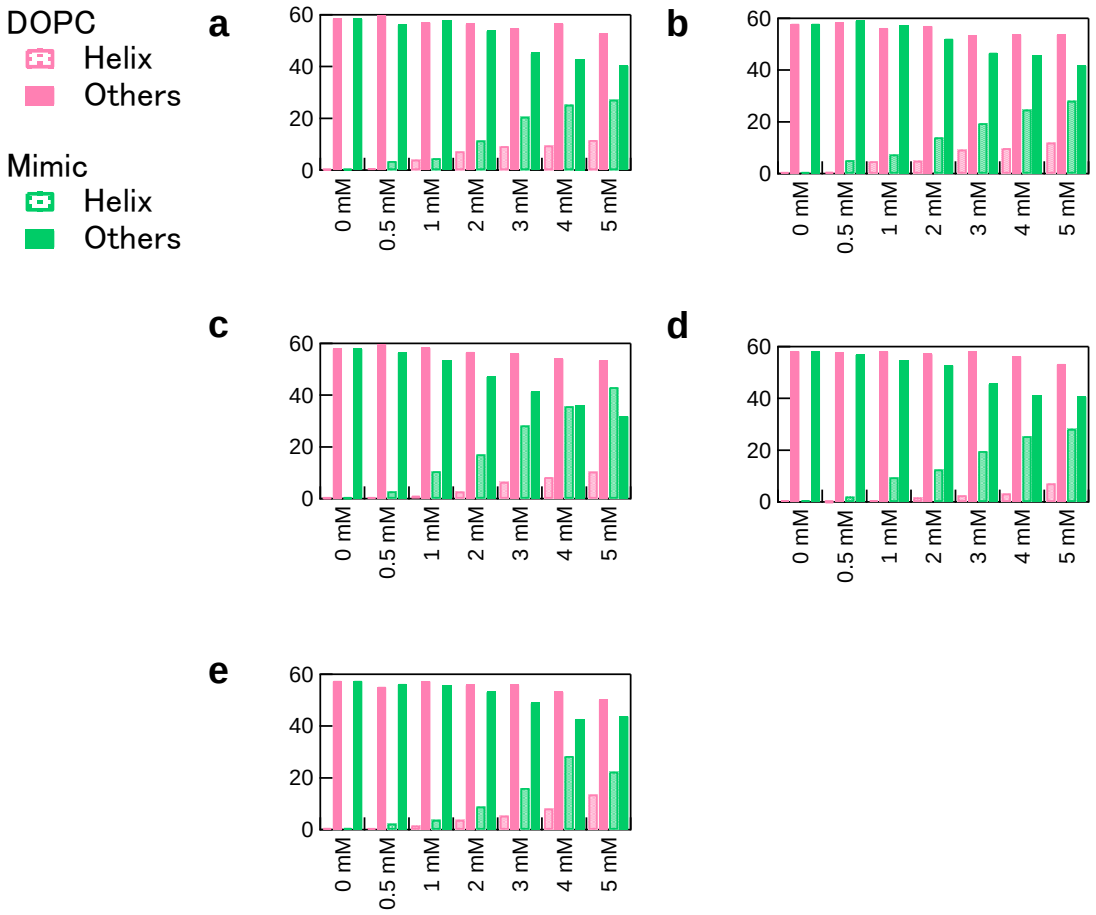

FIGURE 5. The contents of the initial secondary structures of aSN at the various concentration of lipids. *a*-*e*) The amount of α-helix (solid bars) and the other secondary structures (empty bars) for αSN_{WT} (*a*), αSN_{A53T} (*b*), αSN_{103} (*c*), αSN_{129} (*d*), and αSN_{NC} (*e*) at the various concentration of lipids (0 to 5 mM) for DOPC (red bars) and Mimic SUVs (green bars) were predicted by BESTSEL (110) and represented by percentages.

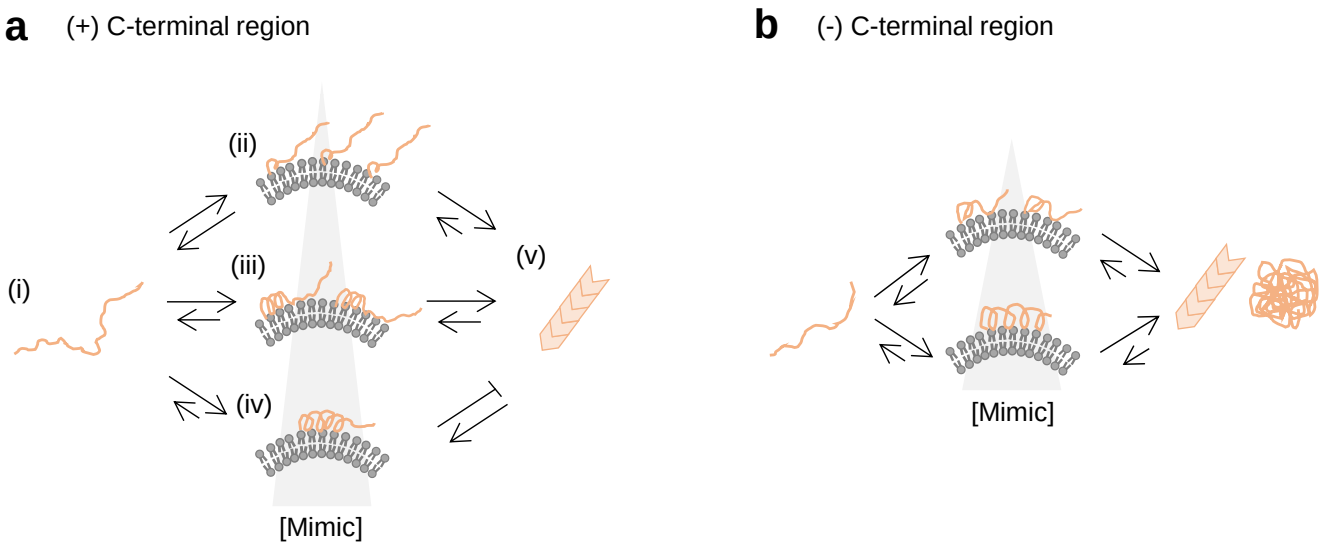

FIGURE 6. The models of the pathway of the fibrillation of αSN in the presence of Mimic vesicles. *a*) The model of αSN including more than half of the C-terminal region. (i) Monomers dissolve in the solution and are fluctuated. (ii-iv) proteins interact with vesicles in a concentration of lipids dependent manner. Proteins of (ii) and (iii) states can form amyloid fibrils (v). The state of (iv) inhibits the fibrillation. *b*) The model of αSN lacked the C-terminal region. The binding of this type protein to vesicles depends on the concentration of lipids, but the fibrillation is not affected. Due to intermolecular strong hydrophobic interaction, proteins tend to form not only amyloid fibrils but also amorphous aggregates.

Chapter 4. Conclusions

Demonstration of the underlying mechanisms of amyloid fibril formation is still challenging, a lot of general aspects on amyloidogenesis have been revealed. Disruption of membranes, which are critical to maintain cell homeostasis, leads to the cell death. Synergetic effects between amyloidogenesis and cytotoxicity through interactions of the amyloidogenic peptide and proteins should be clarified.

In this thesis, based on the physiological and pathological relevance, I showed the effects of lipid membranes on the formation of amyloid fibrils of Aβ peptides and αSN proteins. Generally, depending on the composition of lipids and other components such as shape, temperature, and pressure, physicochemical parameters of lipid membranes (cf. surface charges, fluidity, packing defects, and phase transitions of lipid membranes) are change (112). Thus, these properties altered interactions with the peptide and proteins and their behaviors of aggregation thorough distinct initial conformational states on membranes.

In the second chapter, I revealed that Aβ (1-40) peptides interacted with DOPC SUVs which carried no net charge on their surfaces at the various degree of curvature. Although distinct degrees of curvature did not change the initial random coil-like conformations of Aβ (1-40) peptides, the aggregation behaviors depended on curvature. The high curvature of DOPC SUVs with high packing defects efficiently promoted the formation

of amyloid fibrils of Aβ (1-40) peptides. On the other hand, at low curvature, the fibrillation of Aβ (1-40) peptides was inhibited by forming amorphous aggregates. Thus, packing defects played an important role in acceleration of the formation of amyloid fibrils of Aβ (1-40).

In the third chapter, I showed that the initial conformations of αSN depended on the surface charges between DOPC and Mimic SUVs and a critical factor to determine amyloidogenicity of αSN. αSN could sense the differences in surface charges and alter their conformations to more stabilized states. The high degree of α-helical structures kept to their initial conformations even after long incubation with ultrasonic treatment. However, the low degree of α-helical structures showed the efficient formation of amyloid fibrils. Interestingly, C-terminal charge deleted mutants with α-helical structures showed the formation of amyloid fibrils, which indicated that the charged state and length of unfolded proteins should be also considered in amyloidogenesis.

Although Aβ and αSN are definitely different proteins, co-accumulations of both proteins are detected *in vivo*. Moreover, Aβ enhances the aggregation and accumulation of αSN in brains (113). Thus, recent studies claim that Alzheimer's disease and Parkinson's disease are mutually linked and the study on the mechanisms of the aggregation behaviors of either Aβ or αSN in the presence of both proteins under the biologically more relevant

conditions such as the presence of model membranes is required.

Finally, I expect that my study is helpful to understand the mechanisms of amyloid fibrillation under the conditions where biological membranes interact with aggregation-prone proteins.

References

1. Tycko, R. (2015) Amyloid Polymorphism: Structural Basis and Neurobiological Relevance. *Neuron* **86**, 632-645
2. Knowles, T. P., Vendruscolo, M., and Dobson, C. M. (2014) The amyloid state and its association with protein misfolding diseases. *Nat Rev Mol Cell Biol* **15**, 384-396
3. Astbury, W. T., Dickinson, S. (1935) The X-ray interpretation of denaturation and the structure of the seed globulins. *Biochem J.* **29**, 2351-2360
4. Eanes, E. D., Glenner, G. G. 1968. *J Histichem Cytochem.* **16**, 673-677
5. Eisenberg, D., and Jucker, M. (2012) The amyloid state of proteins in human diseases. *Cell* **148**, 1188-1203
6. Tycko, R. (2011) Solid-state NMR studies of amyloid fibril structure. *Annu Rev Phys Chem* **62**, 279-299
7. Naiki, H., Higuchi, K., Hosokawa, M., and Takeda, T. (1989) Fluorometric Determination of Amyloid Fibrils in Vitro Using the Fluorescent Dye, Thioflavine T. *Anal Biochem.* **177**, 224-249
8. Dobson, C. M. (2003) Protein folding and misfolding. *Nature* **426**, 884-890
9. Selkoe, D. J. (2003) Folding proteins in fatal ways. *Nature* **426**, 900-904
10. Lin, Y., Lee, Y. H., Yoshimura, Y., Yagi, H., and Goto, Y. (2014) Solubility and supersaturation-dependent protein misfolding revealed by ultrasonication. *Langmuir* **30**, 1845-1854
11. Stefani, M., and Dobson, C. M. (2003) Protein aggregation and aggregate toxicity: new insights into protein folding, misfolding diseases and biological evolution. *Journal of molecular medicine* **81**, 678-699
12. Butterfield, S. M., and Lashuel, H. A. (2010) Amyloidogenic protein-membrane interactions: mechanistic insight from model systems. *Angew Chem Int Ed Engl* **49**, 5628-5654
13. Yanagisawa, K., Odaka, A., Suzuki, N., and Ihara, Y. (1995) GM1 ganglioside-bound amyloid β-protein (Aβ): A possible form of preamyloid in Alzheimer's disease. *Nature Medicine* **1**, 1062-1066
14. Pranke, I. M., Morello, V., Bigay, J., Gibson, K., Verbavatz, J. M., Antonny, B., and Jackson, C. L. (2011) alpha-Synuclein and ALPS motifs are membrane curvature sensors whose contrasting chemistry mediates selective vesicle binding. *The Journal of cell biology* **194**, 89-103

15. Pfefferkorn, C. M., Jiang, Z., and Lee, J. C. (2012) Biophysics of alpha-synuclein membrane interactions. *Biochimica et biophysica acta* **1818**, 162-171
16. Hardy, J., and Selkoe, D. J. (2002) The amyloid hypothesis of Alzheimer's disease: progress and problems on the road to therapeutics. *Science* **297**, 353-356
17. Peter Seubert, Tilman Oltersdorf, Michael G. Lee, Robinson Barbour, Cheryl Blomquist, Davis, D. L., Karin Bryant, Lawrence C. Fritz, D. G., Leon J. Thal, Ivan Lieberburg, and Schenk, D. (1993) Secretion of β-amyloid precursor protein cleaved at the amino terminus of the β-amyloid peptide. *Nature* **361**
18. LaFerla, F. M., Green, K. N., and Oddo, S. (2007) Intracellular amyloid-beta in Alzheimer's disease. *Nature reviews. Neuroscience* **8**, 499-509
19. Hu, X., Crick, S. L., Bu, G., Frieden, C., Pappu, R. V., and Lee, J. M. (2009) Amyloid seeds formed by cellular uptake, concentration, and aggregation of the amyloid-beta peptide. *Proceedings of the National Academy of Sciences of the United States of America* **106**, 20324-20329
20. Christian Haass, Michael G. Schlossmacher, Albert Y. Hung, Carmen Vigo-Pelfrey, Angela Mellon, Mrth L. Ostaszewski, Ivan Lieberburg, Edward H. Koo, Dale Schenk, David B. Teplow, and Selkoe, D. J. (1992) Amyloid b-peptide is produced by cultured cells during normal metabolism. *Nature* **359**, 322-325
21. Yagi, H., Hasegawa, K., Yoshimura, Y., and Goto, Y. (2013) Acceleration of the depolymerization of amyloid beta fibrils by ultrasonication. *Biochimica et biophysica acta* **1834**, 2480-2485
22. Cohen, S. I. A., Linse, S., Luheshi, L. M., Hellstrand, E., White, D. A., Rajah, L., Otzen, D. E., Vendruscolo, M., Dobson, C. M., and Knowles, T. P. J. (2013) Proliferation of amyloid-β42 aggregates occurs through a secondary nucleation mechanism. *Proceedings of the National Academy of Sciences of the United States of America* **110**, 9758-9763
23. Matsuzaki, K. (2007) Physicochemical interactions of amyloid beta-peptide with lipid bilayers. *Biochimica et biophysica acta* **1768**, 1935-1942
24. Bisaglia, M., Mammi, S., and Bubacco, L. (2009) Structural insights on physiological functions and pathological effects of alpha-synuclein. *FASEB J* **23**, 329-340
25. Maroteaux, L., Campanelli, J. T., Scheller, R. H. (1988) Synuclein: a neuron-specific protein localized to the nucleus and presynaptic nerve terminal. *The Journal of Neuroscience* **8**, 2804-2815

26. Yu, S., Li, X., Liu, G., Han, J., Zhang, C., Li, Y., Xu, S., Liu, C., Gao, Y., Yang, H., Ueda, K., and Chan, P. (2007) Extensive nuclear localization of alpha-synuclein in normal rat brain neurons revealed by a novel monoclonal antibody. *Neuroscience* **145**, 539-555
27. Ferreon, A. C., Gambin, Y., Lemke, E. A., and Deniz, A. A. (2009) Interplay of alpha-synuclein binding and conformational switching probed by single-molecule fluorescence. *Proceedings of the National Academy of Sciences of the United States of America* **106**, 5645-5650
28. Fusco, G., De Simone, A., Gopinath, T., Vostrikov, V., Vendruscolo, M., Dobson, C. M., and Veglia, G. (2014) Direct observation of the three regions in alpha-synuclein that determine its membrane-bound behaviour. *Nat Commun* **5**, 3827
29. Davidson, W. S. (1998) Stabilization of alpha -Synuclein Secondary Structure upon Binding to Synthetic Membranes. *The Journal of biological chemistry* **273**, 9443-9449
30. Zhu, M., and Fink, A. L. (2003) Lipid binding inhibits alpha-synuclein fibril formation. *The Journal of biological chemistry* **278**, 16873-16877
31. Ohhashi, Y., Kihara, M., Naiki, H., and Goto, Y. (2005) Ultrasonication-induced amyloid fibril formation of β_2-microglobulin. *The Journal of biological chemistry* **280**, 32843-32848
32. So, M., Yagi, H., Sakurai, K., Ogi, H., Naiki, H., and Goto, Y. (2011) Ultrasonication-dependent acceleration of amyloid fibril formation. *J Mol Biol* **412**, 568-577
33. Halverson, K., Fraser, P. E., Kirschner, D. A., and Peter T. Lansbury, J. (1990) Molecular Determinants of Amyloid Deposition in Alzheimer's Disease: Conformational Studies of Synthetic β-Protein Fragments. *Biochemistry* **29**, 2639-2644
34. LOMAKIN, L., CHUNG, D. S., BENEDEK, G. B., KIRSCHNER, D. A., and B.TEPLOW, D. (1996) On the nucleation and growth of amyloid β-protein fibrils: Detection of nuclei and quantitation of rate constants. *Proceedings of the National Academy of Sciences of the United States of America* **93**, 1125-1129
35. Bemporad, F., and Chiti, F. (2012) Protein misfolded oligomers: experimental approaches, mechanism of formation, and structure-toxicity relationships. *Chem Biol* **19**, 315-327

36. Vivekanandan, S., Brender, J. R., Lee, S. Y., and Ramamoorthy, A. (2011) A partially folded structure of amyloid-beta(1-40) in an aqueous environment. *Biochemical and biophysical research communications* **411**, 312-316

37. Aisenbrey, C., Borowik, T., Bystrom, R., Bokvist, M., Lindstrom, F., Misiak, H., Sani, M. A., and Grobner, G. (2008) How is protein aggregation in amyloidogenic diseases modulated by biological membranes? *European biophysics journal : EBJ* **37**, 247-255

38. Bokvist, M., and Grobner, G. (2007) Misfolding of Amyloidogenic Proteins at Membrane Surfaces: The Impact of Macromolecular Crowding. *Journal of the American Chemical Society* **129**, 14848-14849

39. Gorbenko, G. P., and Kinnunen, P. K. (2006) The role of lipid-protein interactions in amyloid-type protein fibril formation. *Chemistry and physics of lipids* **141**, 72-82

40. Rushworth, J. V., and Hooper, N. M. (2010) Lipid Rafts: Linking Alzheimer's Amyloid-beta Production, Aggregation, and Toxicity at Neuronal Membranes. *International journal of Alzheimer's disease* **603052**, 1-14

41. Kakio, A., Nishimoto, S. I., Yanagisawa, K., Kozutsumi, Y., and Matsuzaki, K. (2001) Cholesterol-dependent formation of GM1 ganglioside-bound amyloid beta-protein, an endogenous seed for Alzheimer amyloid. *The Journal of biological chemistry* **276**, 24985-24990

42. Katsumi Matsuzaki, and Horikiri, C. (1999) Interactions of Amyloid β-Peptide (1-40) with Ganglioside-Containing Membranes. *Biochemistry* **38**, 4137-4142

43. Sciacca, M. F., Kotler, S. A., Brender, J. R., Chen, J., Lee, D. K., and Ramamoorthy, A. (2012) Two-step mechanism of membrane disruption by Abeta through membrane fragmentation and pore formation. *Biophys J* **103**, 702-710

44. Hamada, T., Morita, M., Kishimoto, Y., Komatsu, Y., Vestergaard, M. d., and Takagi, M. (2010) Biomimetic Microdroplet Membrane Interface: Detection of the Lateral Localization of Amyloid beta Peptides. *The Journal of Physical Chemistry Letters* **1**, 170-173

45. Morita, M., Hamada, T., Tendo, Y., Hata, T., Vestergaard, M. d. C., and Takagi, M. (2012) Selective localization of Alzheimer's amyloid beta in membrane lateral compartments. *Soft Matter* **8**, 2816-2819

46. Kotler, S. A., Walsh, P., Brender, J. R., and Ramamoorthy, A. (2014) Differences between amyloid-beta aggregation in solution and on the membrane: insights into elucidation of the mechanistic details of Alzheimer's disease. *Chemical Society reviews*

47. Reynolds, N. P., Soragni, A., Rabe, M., Verdes, D., Liverani, E., Handschin, S., Riek, R., and Seeger, S. (2011) Mechanism of membrane interaction and disruption by alpha-synuclein. *Journal of the American Chemical Society* **133**, 19366-19375
48. Sasahara, K., Morigaki, K., Okazaki, T., and Hamada, D. (2012) Binding of islet amyloid polypeptide to supported lipid bilayers and amyloid aggregation at the membranes. *Biochemistry* **51**, 6908-6919
49. Brender, J. R., Salamekh, S., and Ramamoorthy, A. (2012) Membrane Disruption and Early Events in the Aggregation of the Diabetes Related Peptide IAPP from a Molecular Perspective. *Acc. Chem. Res.* **45**, 454-462
50. Pfefferkorn, C. M., Heinrich, F., Sodt, A. J., Maltsev, A. S., Pastor, R. W., and Lee, J. C. (2012) Depth of alpha-synuclein in a bilayer determined by fluorescence, neutron reflectometry, and computation. *Biophysical journal* **102**, 613-621
51. Knight, J. D., and Miranker, A. D. (2004) Phospholipid catalysis of diabetic amyloid assembly. *Journal of molecular biology* **341**, 1175-1187
52. Mizuno, N., Varkey, J., Kegulian, N. C., Hegde, B. G., Cheng, N., Langen, R., and Steven, A. C. (2012) Remodeling of lipid vesicles into cylindrical micelles by alpha-synuclein in an extended alpha-helical conformation. *The Journal of biological chemistry* **287**, 29301-29311
53. Jiang, Z., de Messieres, M., and Lee, J. C. (2013) Membrane Remodeling by alpha-Synuclein and Effects on Amyloid Formation. *Journal of the American Chemical Society* **135**, 15970-15973
54. Pieter E. S. Simith, Jeffrey R. Brender, and Ramamoorthy, A. (2008) Induction of Negative Curvature as a Mechanism of Cell Toxicity by Amyloidogenic Peptides: The Case of Oslet Amyloid Polypeptide. *Journal of the American Chemical Society* **131**, 4470-4478
55. Sun, Y., Lee, C. C., Chen, T. H., and Huang, H. W. (2010) Kinetic process of beta-amyloid formation via membrane binding. *Biophysical journal* **99**, 544-552
56. Ambroggio, E. E., Kim, D. H., Separovic, F., Barrow, C. J., Barnham, K. J., Bagatolli, L. A., and Fidelio, G. D. (2005) Surface behavior and lipid interaction of Alzheimer β-amyloid peptide 1-42: a membrane-disrupting peptide. *Biophysical journal* **88**, 2706-2713
57. Pannuzzo, M., Milardi, D., Raudino, A., Karttunen, M., and La Rosa, C. (2013) Analytical model and multiscale simulations of Aβ peptide aggregation in lipid membranes: towards a unifying description of conformational transitions,

oligomerization and membrane damage. *Physical Chemistry Chemical Physics* **15**, 8940-8952

58. Qu, L., Akbergenova, Y., Hu, Y., and Schikorski, T. (2009) Synapse-to-synapse variation in mean synaptic vesicle size and its relationship with synaptic morphology and function. *The Journal of comparative neurology* **514**, 343-352
59. Abha Chauhan, Indrani Ray, and Chauhan, V. P. S. (2000) Interaction of Amyloid Beta-Protein with Anionic Phospholipids: Possible Involvement Of Lys28 and C-Terminus Aliphatic Amino Acids. *Neurochemical Research* **25**, 423-429
60. Yagi, H., Ban, T., Morigaki, K., Naiki, H., and Goto, Y. (2007) Visualization and classification of amyloid β supramolecular assemblies. *Biochemistry* **46**, 15009-15017
61. Tomas, S., and Milanesi, L. (2010) Mutual modulation between membrane-embedded receptor clustering and ligand binding in lipid membranes. *Nature chemistry* **2**, 1077-1083
62. J. M. H. Kremer, M. W. J. v. d. Esker, C. Pathmamanoharan, and Wiersema, P. H. (1999) Vesicles Variable Diameter Prepared by a Modified Injection. *Biochemistry* **16**, 3932-3935
63. Yoshimura, Y., Lin, Y., Yagi, H., Lee, Y. H., Kitayama, H., Sakurai, K., So, M., Ogi, H., Naiki, H., and Goto, Y. (2012) Distinguishing crystal-like amyloid fibrils and glass-like amorphous aggregates from their kinetics of formation. *Proceedings of the National Academy of Sciences of the United States of America* **109**, 14446-14451
64. Ban, T., Hamada, D., Hasegawa, K., Naiki, H., and Goto, Y. (2003) Direct observation of amyloid fibril growth monitored by thioflavin T fluorescence. *The Journal of biological chemistry* **278**, 16462-16465
65. Ban, T., and Goto, Y. (2006) Direct Observation of Amyloid Growth Monitored by Total Internal Reflection Fluorescence Microscopy. *Methods Enzymol* **413**, 91-102
66. Chatani, E., Lee, Y. H., Yagi, H., Yoshimura, Y., Naiki, H., and Goto, Y. (2009) Ultrasonication-dependent production and breakdown lead to minimum-sized amyloid fibrils. *Proceedings of the National Academy of Sciences of the United States of America* **106**, 11119-11124
67. Paravastu, A. K., Leapman, R. D., Yau, W. M., and Tycko, R. (2008) Molecular structural basis for polymorphism in Alzheimer's beta-amyloid fibrils. *Proc Natl Acad Sci U S A* **105**, 18349-18354

68. Ban, T., Hoshino, M., Takahashi, S., Hamada, D., Hasegawa, K., Naiki, H., and Goto, Y. (2004) Direct observation of Aβ amyloid fibril growth and inhibition. *J Mol Biol* **344**, 757-767

69. Joseph T. Jarrett, Elizabeth P. Berger, and Peter T. Lansbury, J. (1993) The Carboxy Terminus of the β Amyloid Protein Is Critical for the Seeding of Amyloid Formation: Implications for the Pathogenesis of Alzheimer's Disease. *Biochemistry* **32**, 4693-4697

70. Yagi-Utsumi, M., Matsuo, K., Yanagisawa, K., Gekko, K., and Kato, K. (2010) Spectroscopic Characterization of Intermolecular Interaction of Amyloid beta Promoted on GM1 Micelles. *International journal of Alzheimer's disease* **925073**, 1-8

71. Shimanouchi, T., Sasaki, M., Hiroiwa, A., Yoshimoto, N., Miyagawa, K., Umakoshi, H., and Kuboi, R. (2011) Relationship between the mobility of phosphocholine headgroups of liposomes and the hydrophobicity at the membrane interface: a characterization with spectrophotometric measurements. *Colloids and surfaces. B, Biointerfaces* **88**, 221-230

72. Goto, Y., and Fink, A. L. (1989) Conformational states of β-lactamase: molten-globule states at acidic and alkaline pH with high salt. *Biochemistry* **28**, 945-952

73. Lorenzen, N., Nielsen, S. B., Yoshimura, Y., Vad, B. S., Andersen, C. B., Betzer, C., Kaspersen, J. D., Christiansen, G., Pedersen, J. S., Jensen, P. H., Mulder, F. A., and Otzen, D. E. (2014) How Epigallocatechin Gallate Can Inhibit alpha-Synuclein Oligomer Toxicity in Vitro. *The Journal of biological chemistry* **289**, 21299-21310

74. Jarrett, J. T., and Lansbury, P. T., Jr. (1993) Seeding "one-dimensional crystallization" of amyloid: a pathogenic mechanism in Alzheimer's disease and scrapie? *Cell* **73**, 1055-1058

75. Harper, J. D., and Lansbury, P. T., Jr. (1997) Models of amyloid seeding in Alzheimer's disease and scrapie: mechanistic truths and physiological consequences of the time-dependent solubility of amyloid proteins. *Annu Rev Biochem* **66**, 385-407

76. Wetzel, R. (2006) Kinetics and thermodynamics of amyloid fibril assembly. *Acc Chem Res* **39**, 671-679

77. Platt, G. W., Routledge, K. E., Homans, S. W., and Radford, S. E. (2008) Fibril growth kinetics reveal a region of β2-microglobulin important for nucleation and elongation of aggregation. *J Mol Biol* **378**, 251-263

78. Giehm, L., and Otzen, D. E. (2010) Strategies to increase the reproducibility of protein fibrillization in plate reader assays. *Anal Biochem* **400**, 270-281
79. Yoshimura, Y., So, M., Yagi, H., and Goto, Y. (2013) Ultrasonication: an efficient agitation for accelerating the supersaturation-limited amyloid fibrillation of proteins. *Jpn J Appl Phys* **52**, 07HA01-01-07HA01-08
80. Ban, T., Morigaki, K., Yagi, H., Kawasaki, T., Kobayashi, A., Yuba, S., Naiki, H., and Goto, Y. (2006) Real-time and single fibril observation of the formation of amyloid β spherulitic structures. *J Biol Chem* **281**, 33677-33683
81. Gellermann, G. P., Appel, T. R., Tannert, A., Radestock, A., Hortschansky, P., Schroeckh, V., Leisner, C., Lutkepohl, T., Shtrasburg, S., Rocken, C., Pras, M., Linke, R. P., Diekmann, S., and Fandrich, M. (2005) Raft lipids as common components of human extracellular amyloid fibrils. *Proceedings of the National Academy of Sciences of the United States of America* **102**, 6297-6302
82. Goedert, M. (2001) Alpha-synuclein and neurodegenerative diseases. *Nature reviews. Neuroscience* **2**, 492-501
83. Uversky, V. N., Li, J., and Fink, A. L. (2001) Evidence for a partially folded intermediate in alpha-synuclein fibril formation. *The Journal of biological chemistry* **276**, 10737-10744
84. Ikenoue, T., Lee, Y. H., Kardos, J., Saiki, M., Yagi, H., Kawata, Y., and Goto, Y. (2014) Cold denaturation of alpha-synuclein amyloid fibrils. *Angew Chem Int Ed Engl* **53**, 7799-7804
85. Miotto, M. C., Valiente-Gabioud, A. A., Rossetti, G., Zweckstetter, M., Carloni, P., Selenko, P., Griesinger, C., Binolfi, A., and Fernandez, C. O. (2015) Copper binding to the N-terminally acetylated, naturally occurring form of alpha-synuclein induces local helical folding. *Journal of the American Chemical Society* **137**, 6444-6447
86. Crowther, R. A., Jales, R., Spillantini, M. G., Goedert, M. (1998) Synthetic filaments assembled from C-terminally truncated α-synuclein. *FEBS Letters* **436**, 309-312
87. Izawa, Y., Tateno, H., Kameda, H., Hirakawa, K., Hato, K., Yagi, H., Hongo, K., Mizobata, T., and Kawata, Y. (2012) Role of C-terminal negative charges and tyrosine residues in fibril formation of alpha-synuclein. *Brain Behav* **2**, 595-605
88. Kim, T. D., Paik, S. R., Yang, C. H. (2002) Structural and functional implications of C-terminal regions of α-synuclein. *Biochemistry* **41**, 13782-13790

89. Conway, K. A., Harper, J. D., and Lansbury, P. T. (1998) Accelerated in vitro fibril formation by a mutant α-synuclein linked to early-onset Parkinson disease. *Nat Med.* **4**, 1318-1320

90. Conway, K. A., Lee, S.J., Rochet, J.C., Ding, T.T., Wiliamson, R. E., and Lansbury, P. T. Jr. (2000) Acceleration of oligomerization, not fibrillization, is a shared property of both α-synuclein mutations linked to early-onset Parkinson's disease: Implications for pathogenesis and therapy. *Proceedings of the National Academy of Sciences of the United States of America* **97**, 571-576

91. Ferreon, A. C., Moran, C. R., Ferreon, J. C., and Deniz, A. A. (2010) Alteration of the alpha-synuclein folding landscape by a mutation related to Parkinson's disease. *Angew Chem Int Ed Engl* **49**, 3469-3472

92. Polymeropoulos, M. H., Lavedan, C., Leroy, E., Ide, S. E., Dehejia, A., Dutra, A., Pike, B., Root, H., Rubenstein, J., Boyer, R., Stenroos. E. S., Chandrasekharappa, T., Athanassiadou, A., Papapetropoulos, T., Johnson, W. G., Lazzarini, A. M., Duvoisin R. C., Iorio, G. D., Golbe, L. I., and Nussbaum, R. L. (1997) Mutation in the α-synuclein gene identified in families with Parkinson's disease. *Science* **276**, 2045-2047

93. Burre, J., Sharma, M., Tsetsenis, T., Buchman, V., Etherton, M. R., and Sudhof, T. C. (2010) Alpha-synuclein promotes SNARE-complex assembly in vivo and in vitro. *Science* **329**, 1663-1667

94. Snead, D., and Eliezer, D. (2014) Alpha-synuclein function and dysfunction on cellular membranes. *Exp Neurobiol* **23**, 292-313

95. Rosa, D. G., Sant'Angelo, A., Trinchese, F., Arancio, O. (2003) α-synuclein: between synaptic function and dysfunction. *Histology and Histopathology* **2003**, 1257-1266

96. Volpicelli-Daley, L. A., Luk, K. C., Patel, T. P., Tanik, S. A., Riddle, D. M., Stieber, A., Meaney, D. F., Trojanowski, J. Q., and Lee, V. M. (2011) Exogenous alpha-synuclein fibrils induce Lewy body pathology leading to synaptic dysfunction and neuron death. *Neuron* **72**, 57-71

97. Gai, W. P., Yuan, H. X., Li, X. Q., Power, J. T., Blumbergs, P. C., and Jensen, P. H. (2000) In situ and in vitro study of colocalization and segregation of alpha-synuclein, ubiquitin, and lipids in Lewy bodies. *Exp Neurol* **166**, 324-333

98. Vamvaca, K., Volles, M. J., and Lansbury, P. T., Jr. (2009) The first N-terminal amino acids of alpha-synuclein are essential for alpha-helical structure formation in vitro and membrane binding in yeast. *Journal of molecular biology* **389**, 413-424

99. Qin, Z., Hu, D., Han, S., Hong, D. P., Fink, A. L. (2007) Role of different regions of α-synuclesin in the assembly of fibrils. *Biochemistry* **46**, 13322-13330

100. Jao, C. C., Hegde, B. G., Chen, J., Haworth, I. S., and Langen, R. (2008) Structure of membrane-bound alpha-synuclein from site-directed spin labeling and computational refinement. *Proceedings of the National Academy of Sciences of the United States of America* **105**, 19666-19671

101. Shvadchak, V. V., Yushchenko, D. A., Pievo, R., and Jovin, T. M. (2011) The mode of alpha-synuclein binding to membranes depends on lipid composition and lipid to protein ratio. *FEBS Lett* **585**, 3513-3519

102. Takamori, S., Holt, M., Stenius, K., Lemke, E. A., Gronborg, M., Riedel, D., Urlaub, H., Schenck, S., Brugger, B., Ringler, P., Muller, S. A., Rammner, B., Grater, F., Hub, J. S., De Groot, B. L., Mieskes, G., Moriyama, Y., Klingauf, J., Grubmuller, H., Heuser, J., Wieland, F., and Jahn, R. (2006) Molecular anatomy of a trafficking organelle. *Cell* **127**, 831-846

103. Anderson, V. L., Ramlall, T. F., Rospigliosi, C. C., Webb, W. W., and Eliezer, D. (2010) Identification of a helical intermediate in trifluoroethanol-induced alpha-synuclein aggregation. *Proceedings of the National Academy of Sciences of the United States of America* **107**, 18850-18855

104. Giehm, L., Oliveira, C. L., Christiansen, G., Pedersen, J. S., and Otzen, D. E. (2010) SDS-induced fibrillation of alpha-synuclein: an alternative fibrillation pathway. *Journal of molecular biology* **401**, 115-133

105. Eliezer, D. (2013) The mysterious C-terminal tail of alpha-synuclein: nanobody's guess. *Journal of molecular biology* **425**, 2393-2396

106. Galvagnion, C., Buell, A. K., Meisl, G., Michaels, T. C., Vendruscolo, M., Knowles, T. P., and Dobson, C. M. (2015) Lipid vesicles trigger alpha-synuclein aggregation by stimulating primary nucleation. *Nature chemical biology* **11**, 229-234

107. Yagi, H., Kusaka, E., Hongo, K., Mizobata, T., and Kawata, Y. (2005) Amyloid fibril formation of alpha-synuclein is accelerated by preformed amyloid seeds of other proteins: implications for the mechanism of transmissible conformational diseases. *The Journal of biological chemistry* **280**, 38609-38616

108. Szoka, F. J. (1980) Comparative properties and methods of preparation of lipid vesicles (liposomes). *Annu Rev Biophys Bioeng.* **9**, 467-508

109. Jo, E., McLaurin, J., Yip, C. M., St George-Hyslop, P., and Fraser, P. E. (2000) alpha-Synuclein membrane interactions and lipid specificity. *The Journal of biological chemistry* **275**, 34328-34334

110. Micsonai, A., Wien, F., Kernya, L., Lee, Y. H., Goto, Y., Refregiers, M., and Kardos, J. (2015) Accurate secondary structure prediction and fold recognition for circular dichroism spectroscopy. *Proceedings of the National Academy of Sciences of the United States of America* **112**, E3095-3103

111. Wihelm, B., Mandad, S., Truckenbrodt, S., Krohnert, K., Schafer, C., Rammner, B., Koo, S. J., Claben, G. A., Krauss, M., Haucker, V., Urlaub, H., Rizzoli, S. O. (1014) Composition of isolated synaptic boutons reveals the amounts of vesicle trafficking proteins. *Science* **344**, 1023-1028

112. Bigay, J., and Antonny, B. (2012) Curvature, lipid packing, and electrostatics of membrane organelles: defining cellular territories in determining specificity. *Dev Cell* **23**, 886-895

113. Masliah, E., Rockenstein, E., Veinbergs, I., Sagara, Y., Mallory, M., Hashimoto, M., and Mucke, L. (2001) beta-amyloid peptides enhance alpha-synuclein accumulation and neuronal deficits in a transgenic mouse model linking Alzheimer's disease and Parkinson's disease. *Proceedings of the National Academy of Sciences of the United States of America* **98**, 12245-12250

List of publications

Main Paper

Terakawa, M. S., Yagi, H., Adachi, M., Lee, Y.-H., and Goto, Y.

Small Liposomes Accelerate the Fibrillation of Amyloid β (1-40).

The Journal of Biological Chemistry, **290**, 815-826 (2015)

Related paper

Terakawa, M. S., Lin, Y., Ikenoue, T., Fukui, N., Kawata, Y., Lee, Y.-H., and Goto, Y.

Study on the mechanism of amyloidogenesis of α-synuclein on presynaptic membrane mimics.

in preparation